ORNL/SPR-2020/1577

MERCURY REMEDIATION TECHNOLOGY DEVELOPMENT

for Lower East Fork Poplar Creek—FY 2020 Update

OAK RIDGE National Laboratory

ORNL/SPR-2020/1577

Mercury Remediation Technology Development

for Lower East Fork Poplar Creek—FY 2020 Update

Teresa J. Mathews
Melanie A. Mayes
Scott C. Brooks
Chris DeRolph
Alexander Johs
Sujith Nair
Leroy Goñez-Rodríguez
Simon Pouil
Louise Stevenson
Amber D. Hills
Paul Matson
José L. Martínez Collado

September 2020

Prepared by
OAK RIDGE NATIONAL LABORATORY
Oak Ridge, Tennessee 37831-6283 managed by
UT-BATTELLE, LLC
for the
US DEPARTMENT OF ENERGY
under contract DE-AC05-00OR22725

Acknowledgments

We would like to thank Janice Hensley and Jimmy Massey of URS | CH2M Oak Ridge LLC and Elizabeth Phillips and Brian Henry of the US Department of Energy's Oak Ridge Office of Environmental Management for their support of mercury technology development in Oak Ridge and their project oversight and support for this document. Additional contributors to various research and technology development activities that provided a basis for the report's evaluations and recommendations include Kenneth Lowe and Michael Jones (Oak Ridge National Laboratory), and Carrie Miller (Ramapo College). VJ Ewing, Kathy Jones, and Olivia Shafer of Oak Ridge National Laboratory were responsible for editing and graphic design work, and their contributions are sincerely appreciated.

Contents

List of Figures

List of Tables

Introduction

Mercury (Hg) remediation is a high priority for the US Department of Energy (DOE) Oak Ridge Office of Environmental Management. Mercury contamination in the environment can be found at all three DOE facilities in Oak Ridge, but probably the greatest environmental risk concern relative to Hg on the Oak Ridge Reservation is associated with historical Hg losses at and near the Y-12 National Security Complex (Y-12). Water and fish from East Fork Poplar Creek (EFPC) downstream of Y-12 exceed regulatory thresholds. Because of the complexities of Hg transport and fate in the aquatic environment, conventional remedial options for EFPC are highly uncertain.

DOE is using a phased adaptive management approach to Hg remediation at Y-12 with a focus in the next few years on construction of the Mercury Treatment Facility (MTF) to treat the most contaminated Y-12 outfall entering EFPC (DOE 2017a; DOE 2017b). Once operational, the MTF will provide additional protection against inadvertent releases of Hg into the stream from decontamination and decommissioning of Y-12 Hg-use buildings. Although the MTF is anticipated to substantially decrease Hg water concentrations and flux in the upper part of EFPC, research and technology development are needed to develop appropriate and long-term remedial solutions for the downstream environment. Since late 2014, the Oak Ridge Office of Environmental Management and URS | CH2M Oak Ridge LLC/Restoration Services, Inc. have supported DOE's Oak Ridge National Laboratory (ORNL) Environmental Sciences Division staff in conducting field and laboratory studies to develop Hg remedial technology solutions for lower EFPC (LEFPC).

A technology development strategy for LEFPC was developed in 2014 that was consistent with the adaptive management paradigm and DOE's technology readiness level (TRL) guidelines (Peterson et al. 2015). Initially, a thorough review of the literature was conducted and site-specific information was collected to develop a broad number of potential technologies that might be applied in LEFPC. An adaptive management approach was then used to focus on technologies that might have the most promise and potential remediation benefit. Field and laboratory studies conducted from 2014 to 2020 have identified the major drivers of Hg flux and bioaccumulation in EFPC and narrowed the list of high-merit technologies that might be of use in remediating the downstream environment.

Whereas previous annual reporting updates for *Mercury Remediation Technology Development for Lower East Fork Poplar Creek* have focused on presenting detailed results from the previous fiscal year, this FY 2020 update takes a comprehensive, higher-level approach to the research and technology development activities conducted since 2014. The report is organized consistent with the three tasks defined in the LEFPC strategic plan (Peterson et al. 2015).

- Task 1, Soil and Groundwater Source Control, focuses on addressing downstream Hg sources to the creek (especially floodplain and bank soils) and groundwater.
- Task 2, Surface Water and Sediment Manipulation, centers on potential manipulation of in-stream processes, including the many water and sediment chemistry factors that affect Hg methylation.
- Task 3, Ecological Manipulation, investigates methods to manipulate the food chain at both lower and higher levels of organization to decrease Hg concentrations in fish.

Together, the three study tasks focus on manipulating the key factors that affect Hg concentrations in fish: the amount of inorganic Hg available to the ecosystem, conversion of inorganic Hg to methylmercury

(MeHg), and bioaccumulation of MeHg through the food web (Figure 1). A major focus of the project has been understanding Hg transport and fate processes in the EFPC system so that targeted, site-specific technologies can be developed. In 2019, a fourth task was added:

- Task 4, Watershed Modeling, integrates data collected from field and laboratory studies from Tasks 1–3 to define conceptual and quantitative models for EFPC to inform future remedial decision-making.

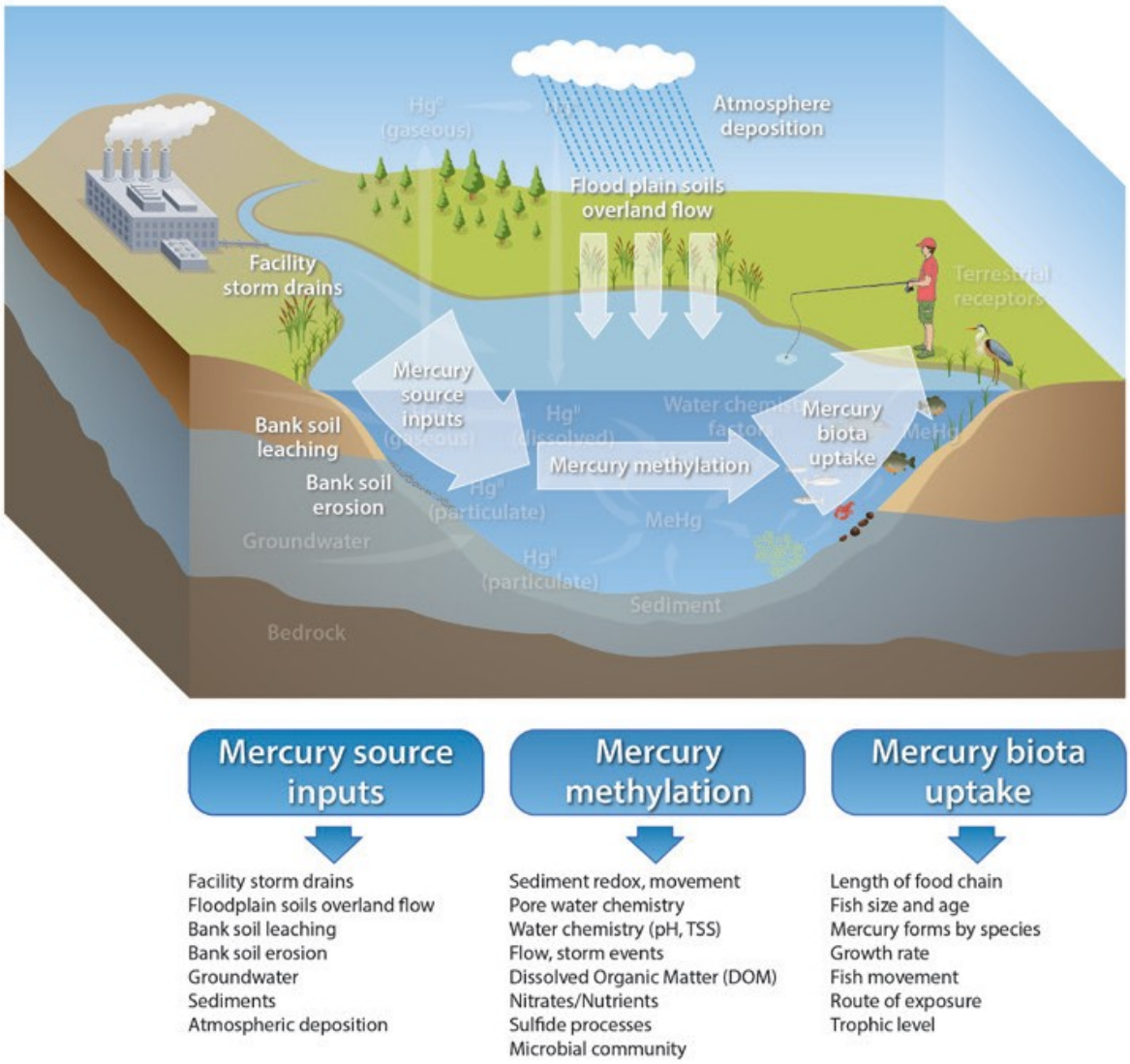

Figure 1. The three major factors affecting Hg concentrations in fish: source inputs to the ecosystem, Hg methylation, and bioaccumulation of MeHg. (TSS = total suspended solids.) (Source: Peterson et al. 2015).

Research and Technology Development Results

Results from the LEFPC Mercury Remediation Technology Development Project in FY 2020, as well as the key findings from previous years, are provided in the following subsections.

Soil Source Control and Engineered Sorbents

SOIL

Field Measurements of Bank Soil Fluxes

In the early 1990s, a remedial action removed more than 34,000 m^3 of floodplain soils with Hg concentrations exceeding 400 mg/kg. More recently, downstream bioaccumulation and biomagnification of Hg in fish continues despite decreasing releases from Y-12, strongly suggesting that processes in the stream and its environs contribute to bioaccumulation. Soils and sediments downstream of Y-12 account for most of the annual export of Hg to the watershed (Watson et al. 2016, 2017). As Hg erodes from bank and floodplain soils, it contributes to the concentration of total Hg in the water column and sediments, where it can be transformed into MeHg by microbes or periphyton (Figure 2). Therefore, providing technologies to reduce the flux of Hg into the creek is the primary goal of this task.

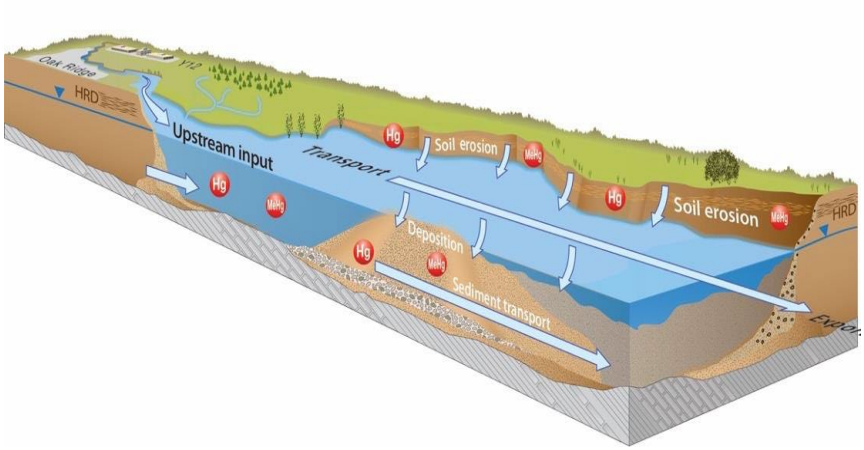

Figure 2. Conceptual diagram of Hg and MeHg release from stream bank soils and incorporation into stream water and streambed sediments. The historical release deposit (HRD) is shown as a distinct layer above the water table. (Source: Peterson et al. 2018)

KEY CONCEPTS

- Improving understanding of Hg dissolution and desorption from creek bank soils
- Eroding floodplain soil banks deliver fluxes of Hg into EFPC
- Reducing Hg fluxes into EFPC should decrease Hg available for methylation
- Developing methods to quantitatively measure erosion from creek bank soils
- Pilot testing engineered sorbent performance in the field

In previous years, the locations of the highest Hg concentrations in stream banks—the historical release deposits (HRDs)—have been identified (Mathews et al. 2019; Dickson et al. 2018). This year, the focus has shifted toward measuring erosion rates, which is a key need for modeling Hg release during storm events. Understanding the spatial and temporal patterns of erosion will provide concrete data with which to test and calibrate the watershed model (Task 4). Quantitative measurements of erosion will enable continued prioritization of stream bank locations for future studies and potential remedial investigations (Figure 3).

Using Lidar to Measure Erosion of Stream Banks

A field-portable terrestrial laser scanning device was recently purchased to provide state-of-the-art erosion measurements of EFPC stream banks. The device, based on lidar (light detection and ranging) technology, can provide similar information to that of the 3D mesh experiment described previously (Mathews et al. 2019). Rather than taking precise distance measurements between a reference point and the creek bank by hand, the lidar instrument can take hundreds of thousands of measurements in minutes. The instrument aims a laser beam at an interior fully rotating mirror that reflects the beam outward, and then measures the return signals to generate 360°, 3D images composed of millions of points (known as a "point cloud"). Over time (for example, the next year or two) the instrument will enable us to also obtain an accurate estimate of the change in volume of the creek bank (i.e., erosion and deposition) being measured at each location. A set of 10 locations (each approximately 10 m wide) at which erosion pin measurements have been occurring for at least 5 years (as detailed in Mathews et al. 2019) were chosen for a pilot study. Erosion pin and mesh measurements have continued throughout FY 2020 and will continue in the future because they constitute an important long-term record of sedimentation processes in EFPC.

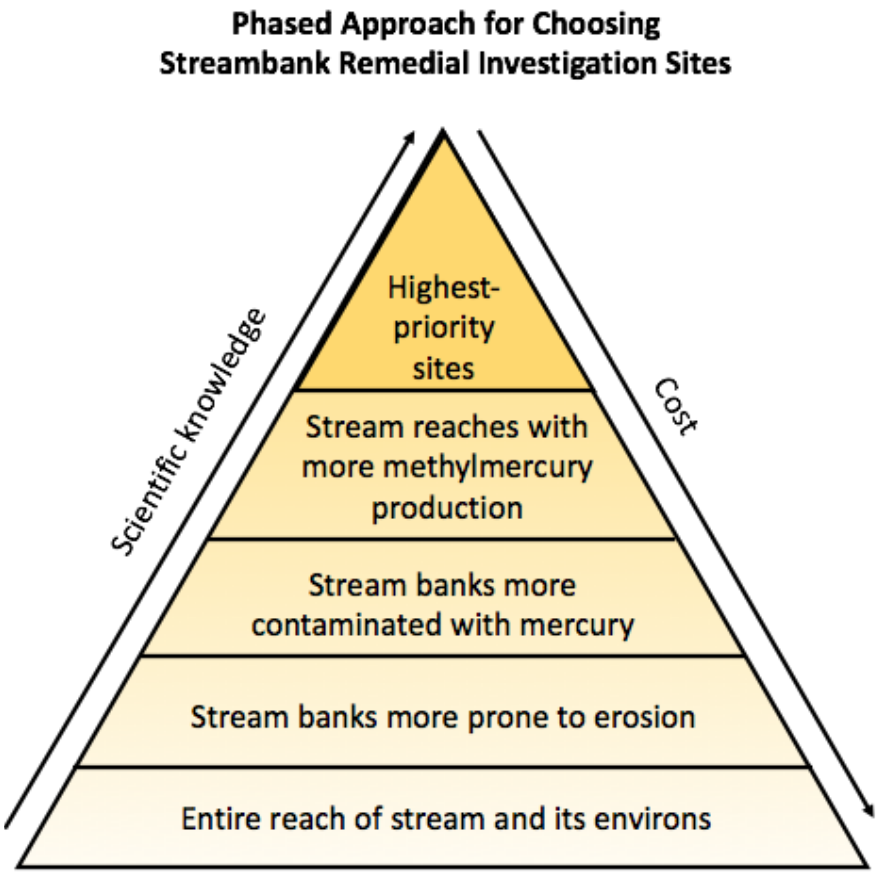

Figure 3. Phased approach for choosing stream bank remedial investigation sites and determining target areas for remediation. (Source: Peterson et al. 2015)

To test this new technology, a series of tests was developed to corroborate that the information from the instrument is reliable. The first test consisted of taking scans of a small area on the soil surface. After taking a scan, a small depression was created and the scan was repeated (Figure 4). Our team is currently testing different software capable of generating high-resolution maps from the lidar point clouds. So far, we generated a 3D model of the soil test. As seen in Figure 5, we cropped the point cloud to focus only on the area analyzed. Figure 5 represents a depth gradient of the depression created in the soil (side view). Software like these will allow us to calculate erosion estimates with much higher precision than using erosion pins or meshes (Mathews et al. 2019). Furthermore, because of the efficiency of data acquisition, we will be able to develop many more measurements of erosion than were possible using erosion pins or meshes. This study will become a major focus during the coming year by analyzing creek banks throughout EFPC (Figure 6). The data will provide improved information to better model erosional and depositional processes in EFPC (Task 4), and to provide improved estimates of Hg input into EFPC.

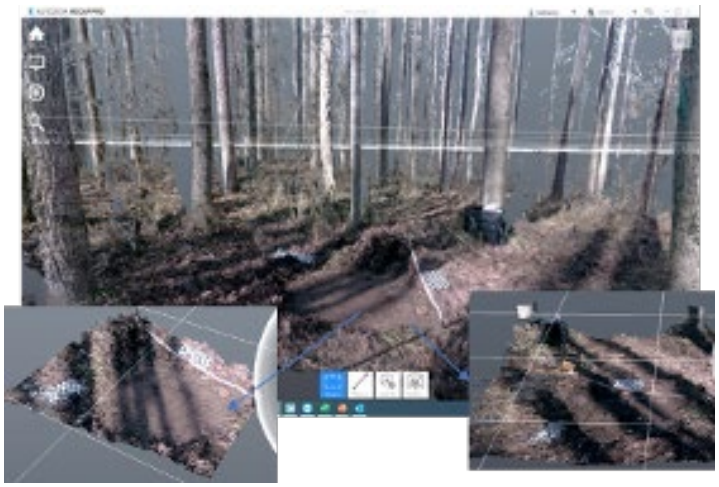

Figure 4. Point cloud of the sampling area used to test the lidar technology.

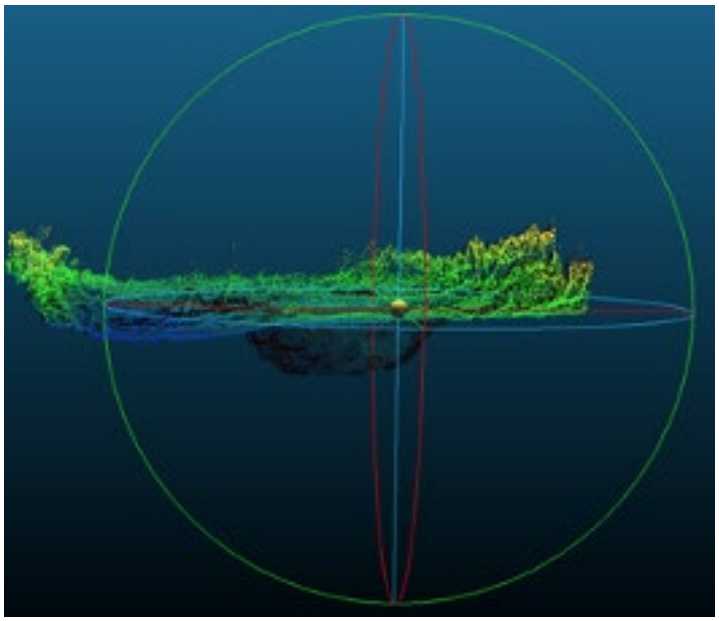

Figure 5. Depth gradient point cloud of a depression in the ground seen from the side.

Figure 6. Locations (in terms of kilometers above the mouth of EFPC) where lidar will be used to measure the configuration of creek banks over time.

Release of Hg from Bank Soils—Laboratory Measurements

Solubility, sorption, and desorption processes control the transport and mobility of Hg species in the environment. The potential release of Hg from EFPC creek banks and specifically the HRD soil layer may contribute disproportionately to elevated Hg levels in downstream environments. Thus, desorption or dissolution of Hg associated with contaminated bank soils may also increase bioavailable Hg and enhance MeHg production in the system.

Two types of Hg-contaminated soils were collected from the creek bank of EFPC at multiple locations to study the release of Hg from EFPC bank soils and to identify conditions that promote the mobilization of Hg (Table 1; Figure 7). Sites in EFPC are represented with the identifier EFPC kilometer (EFK) followed by a number that designates the creek kilometer measured upstream from the mouth of the creek. Regular and HRD layer bank soils were collected from randomly selected locations between EFK 22.46 and 8.41.

Table 1. Sampling locations, EFK distance, and total Hg concentrations of bank soil samples from EPFC.

Sample ID	*EFK*	*Latitude*	*Longitude*	*Total Hg (mg/kg)*	*Type*
2-7	21.30	36.00431	−84.25742	74.0	Bank soil
5-6	18.51	36.00563	−84.28060	56.3	Bank soil
9-8	14.36	35.99090	−84.31233	66.7	Bank soil
16-3	8.41	35.96950	−84.34164	48.2	Bank soil
BL-2	22.46	36.00120	−84.24643	2386	HRD layer
BL-8	19.39	36.00979	−84.27480	1039	HRD layer
BL-18	19.02	36.00900	−84.27892	309	HRD layer
BL-22	18.94	36.00894	−84.27972	819	HRD layer
BL-33	18.49	36.00550	−84.28054	985	HRD layer
BL-43	18.20	36.00420	−84.28268	184	HRD layer
BL-54	17.97	36.00340	−84.28499	447	HRD layer

Figure 74. Locations in EFPC for the collection of contaminated creek bank soils (green = regular soil; purple = HRD layer soil).

EFPC water is carbonate-buffered to a mildly alkaline pH of 7.5–8.0 due to the prevalence of calcium carbonate minerals in the creek bed. Artificial creek water was prepared to mimic the solution chemistry of EFPC. Additionally, natural water was collected from the uncontaminated reference site Hinds Creek with similar water chemistry as EFPC.

EFPC bank soils throughout EFPC are classified as loam and silty loam soils. Although the mean silt fraction and total carbon contents decrease with EFK distance, no other soil components show variability with EFK distance (Dickson et al. 2019). Fine-grained soils are typically associated with greater porosity and particle surface area, which can affect contaminant partitioning and transport processes. Bank soil samples were separated into five size fractions to determine the effect of particle size on total Hg release. Fractionation was carried out by dry sieving the soil samples into five size classes (>2.36, 1.00–2.36, 0.125–1.00, 0.053–0.125, and <0.053 mm). To limit variability from particle size distribution, the experiments focused on the size fraction between 0.125 and 1.00 mm.

Initially, a series of batch experiments was conducted to investigate the relationship between solid-solution ratio and the amount of Hg released from the soils. The artificial creek water and soil were combined at various solid-solution ratios for 24 h under gentle agitation until an equilibrium between the solid and the solution phase was achieved.

The partitioning between solids and solution can be described by the partition coefficient (K_d) and is a key parameter for estimating the release and migration potential of contaminants at aqueous-solid interfaces in the subsurface.

Frequently, the partitioning of contaminants between a solid phase and the aqueous phase is described by an empirical linear model in which the partition coefficient (K_d) describes the relationship between the mass of contaminant per mass of the solid (Q_e) to the contaminant concentration in solution at equilibrium (C_{eq}).

$$K_d = \frac{Q_e}{C_{eq}}$$

Thus, the concentration of Hg in solution is proportional to the amount of Hg sorbed to soil particles and decreases with increasing solid-solution ratios.

The results from the batch experiments show that Hg release from increased with decreasing solid-solution ratios (Figure 8), which is generally consistent with equilibrium partitioning between solid and solution. However, the equilibrium concentration of Hg in solution was found to be disproportionally higher at low solution:solid ratios (Figure 8B). This observation could indicate that the partition coefficient depends on the solution:solid ration, or alternatively, that a fraction of the Hg is desorbed from soil particles as the mass of Hg released from soil increases with decreasing C_{eq} (Figure 8C). Overall, the results of these batch studies suggest that contaminated EFPC bank soils may contain Hg species with variable mobility and that both low and high solution:solid ratios can result in the release of substantial quantities of Hg into the water column. HRD soils constitute the largest reservoir of Hg and should be a priority for remediation efforts.

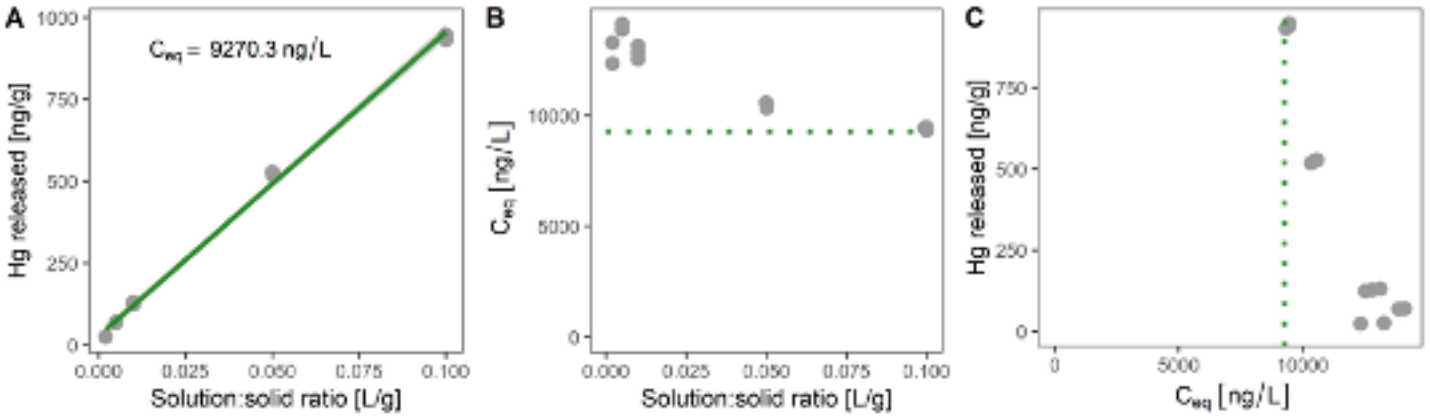

Figure 8. Release of Hg from a selected HRD soil sample (BL-33). (A) Hg released from soil as a function of solution:solid ratio and linear model fit to the data (green solid line). The linear model assumes dissolution of Hg from the sample to a fixed equilibrium concentration (C_{eq}) that is constant over all solution:solid ratios. (B) Experimentally determined equilibrium concentration as a function of solution:solid ratio. (C) Hg released from soil as a function of equilibrium concentration (C_{eq}). The horizontal and vertical green dotted lines indicate the predicted C_{eq} as determined from the linear model fit in (A).

ENGINEERED SORBENTS

Determining the Efficacy of Engineered Sorbents

Soils and sediments can retain Hg contamination for decades, where it is a persistent source that can be mobilized and transformed into MeHg. Sorbent amendments are considered a low-impact alternative to dredging and capping for the remediation of soil and sediments on Hg-contaminated sites (Gilmore et al. 2013); however, the number of field studies involving Hg remediation is still quite small. Engineered sorbents are widely used for the removal of heavy metals from industrial waste streams and for in situ stabilization. While remediation strategies using in situ amendments have been successfully demonstrated for organic contaminants, the application of sorbent amendments for remediation of Hg remains limited. The objective when using sorbents to stabilize contaminants is to reduce the bioavailability of Hg for methylation and MeHg for bioaccumulation. Studies focused on developing technologies for Hg remediation have thus far involved the use of carbon-based functionalized mesoporous silica, organocation-modified clays, and brass sorbents (Paulson et al. 2014, 2018; Johs et al. 2019). Here, we want to determine the effectiveness of various engineered sorbents that can immobilize Hg, considering capacity and efficiency.

Field Sorbent Deployment Experiment

The analyses for the coupons deployed at all three sites were completed for all time points (1 month, 3 months, 6 months, and 1 year). All three sites showed a progression with increasing sorption over time. Sorbents deployed at EFK 22 (National Oceanic and Atmospheric Administration [NOAA]) (Figure 9a) removed 244–1,052 ng Hg/g sorbent (dry weight) using biochar. Activated carbon removed 296–758 ng Hg/g sorbent and sand removed 49–93 ng Hg/g sorbent. Recovery from sand was low, as expected since it represents a control. The coupons deployed at EFK 17.8 (former Bruner's market) (Figure 9b) removed 244–2,080 ng Hg/g sorbent with biochar, 410–1,672 ng Hg/g sorbent with activated carbon, and 39–228 ng Hg/g sorbent with sand. At New Horizon (EFK 8.7) biochar had the highest amount of Hg removed (516–2,620 ng Hg/g sorbent), followed by activated carbon (511–1,350 ng Hg/g) and sand (108–170 ng Hg/g) (Figure 9c). Although we also deployed organoclay, the analyzed Hg concentrations were less than the detection limit, so we assumed that the diffusional properties of the material were incompatible with the experimental configuration.

Interpreting the results is complicated because of the wide range of observed Hg concentrations. Triplicate analyses of each sample were conducted and showed minimal spread of data. However, the analyses of the three replicates deployed to each site demonstrated considerable variation in the data, suggesting that slightly different conditions within each site (e.g., depth of water, burial under sediments, flow rate of the stream, Hg concentrations in the water) are sufficiently different to impart differences in the replicate samples. The replicates were generally located within 15 cm of each other. To have a better understanding of the biogeochemical conditions at the locations where the sorbents were deployed, sediment, water, and biomass samples were collected at each location while retrieving the last set of coupons at 12 months, and analyses are underway. This study will yield specific information to determine the efficacy of the sorbents when deployed in the field. Overall, based on the preliminary results from the coupons deployed on the creek bed, biochar was more efficient for Hg removal, activated carbon had a lower efficiency, and the sand as a control had the lowest removal of Hg.

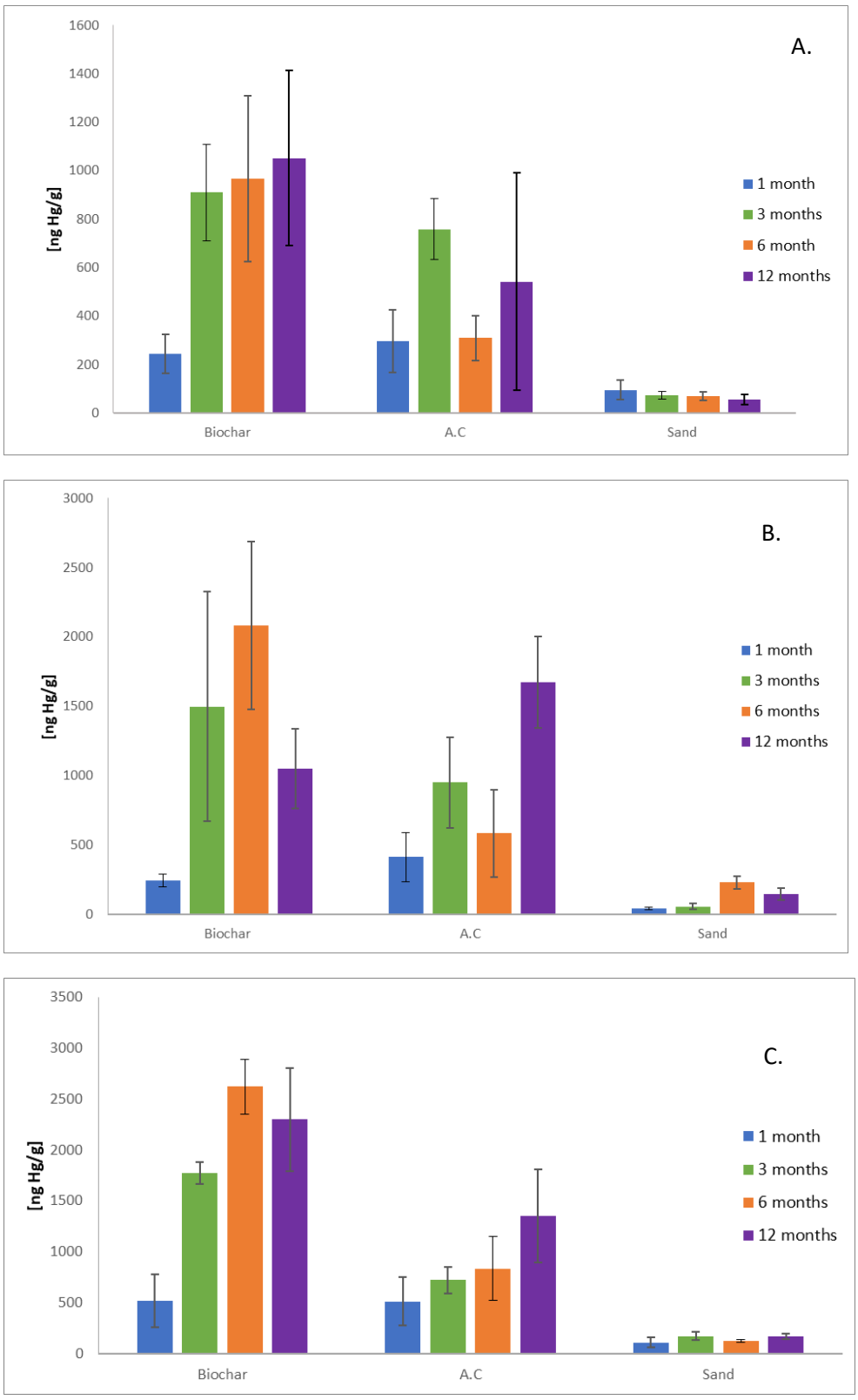

Figure 9. Mercury concentrations in sorbent coupons (biochar, activated carbon [AC], and sand) at 1, 3, 6, and 12 months deployment at (A) NOAA (EFK 22), (B) Bruners (EFK 17.8), and (C) the New Horizon location (EFK 8.7).

Soil Research and Technology Development Needs

In previous years, we identified the areas of the bank soils having the highest Hg and MeHg concentrations and that thus constitute the highest priority for future investigations and potential remedial activities (Mathews et al. 2019; Dickson et al. 2018). In general, the region of the creek banks with the HRD layer have the highest concentrations. Batch studies using contaminated HRD and creek bank soils also demonstrate that the release of Hg from the HRD soils is greater than for the remainder of the creek bank soils, and that a linear dissolution model is appropriate to describe the data. To complete the prioritization triangle (Figure 3), we are now focusing on developing methods to quantify erosion using a sophisticated lidar technique. Eventually, we will be able to connect data of the Hg and MeHg creek bank concentrations, with the potential for desorption (Figure 6) and for erosion to provide a solid basis for identifying the creek banks that are most likely to release Hg. These measurements will aid the conceptual and quantitative watershed modeling task by providing data for calibration and validation of the watershed model.

As described in the 2019 report (Mathews et al. 2019), additional lab-scale studies with the engineered sorbents and real EFPC water are still needed. In general, the chemistry of Hg in EFPC is dominated by complexation with dissolved organic carbon (DOC), which cannot be readily replicated. The presence of DOC induces aqueous complexation with Hg and dramatically decreases the reactivity of Hg with the sorbents. Therefore, a new set of column studies are planned for the Aquatic Ecology Laboratory (AEL) involving the three most promising engineered sorbents and EFPC water, which will enable an improved understanding of long-term sorbent performance under conditions of Hg speciation found in EFPC.

Results from the field deployment of sorbent coupons show that biochar was more effective than activated carbon, and that the coupons continued to adsorb Hg for at least a year after deployment. The remaining analyses of the study are ongoing, which will provide insight into performance at NOAA and Bruner sites (EFK 22 and 18.7), and into the environmental conditions at each site (Hg and MeHg in water, sediments, and periphyton). This study will enable a greater understanding of expected sorbent performance in the EFPC environment.

Overall, we are moving from basic scientific information, such as the distribution of Hg and MeHg and erosion potential, toward the capacity for remediation using engineered sorbents. In future years (beginning in FY 2022), emphasis will be placed on physical technologies that can be deployed to stabilize LEFPC creek banks while also using sorbents to chemically stabilize Hg and MeHg. The costs of the technologies will be an important aspect of these future studies.

Surface Water and Sediment Manipulation

Importance of Surface Water Chemistry

The goal of water chemistry manipulation technologies is to disrupt Hg transport and loading, aqueous partitioning, methylation, and exposure/bioaccumulation mechanisms. By decreasing total Hg and MeHg concentrations in surface water, the expectation is for a decreased flux of these constituents and their concentration in fish tissue. New water chemistry manipulation strategies and technologies are sought to effectively decrease Hg bioavailability and bioaccumulation while limiting effects on the environment or costly soil removals.

Methylmercury is generally assumed to be the form of Hg that is assimilated and bioaccumulated. Although this is true in many nonpolluted sites, in an industrially contaminated setting with very high Hg concentrations, such as EFPC, inorganic Hg could also contribute to Hg body burden (Hines et al. 2000; Horvat et al. 2003). If this is the case, decreasing waterborne Hg concentration should lead to rapid decreases in fish Hg because inorganic Hg is eliminated from tissues more rapidly than MeHg (Trudel and Rasmussen 1997). Therefore, actions targeted at lowering inorganic Hg concentration might directly lower Hg accumulation in EFPC biota in addition to lowering the supply of Hg for methylation by bacteria.

Total Hg concentration in LEFPC surface water exceeds the State of Tennessee's ambient water quality criterion, with the largest percentage of surface water Hg concentrations composed of inorganic Hg bound to particles. Point source discharges of Hg from Y-12 and redistribution and transport of legacy Hg within the watershed (e.g., bank soils,

sediments) were believed to be the largest source of Hg in LEFPC. Nevertheless, the role of current releases of Hg from Y-12 versus downstream legacy sources outside of Y-12 was not well understood and was, therefore, an area of investigation.

Key unknowns concerning the role of surface water chemistry previously identified (Peterson et al. 2015) included the magnitude of Hg and MeHg flux along EFPC. Quantifying flux serves several purposes for site management and technology development, including (1) supporting conceptual model development and site characterization; (2) assessing exposure and risk evaluation; (3) informing site prioritization; (4) informing remediation selection and design; and (5) providing baseline (BL) information for performance, compliance, and long-term monitoring and evaluation. The prevailing conceptual model at the start of this project held that Outfall (OF) 200 discharge was the dominant source of base flow Hg loading to EFPC (Peterson et al. 2015). That might have been the case in the past, but changes in operations (e.g., cessation of the flow management program in mid-2014) and ongoing improvements in water quality in upper EFPC (UEFPC) might have altered the components of the mass balance.

To address these needs and fill knowledge gaps, a new water monitoring station was established at the Wiltshire Drive overpass (EFK 16.2) to supplement existing stations at EFK 5.4 and 23.4 (Station 17). Using stream discharge and concentration data obtained under base flow conditions at each of the three stations, instantaneous material fluxes were calculated.

Our results show that diffuse legacy sources outside of Y-12 make substantial contributions to Hg flux along EFPC. Additionally, we demonstrated that MeHg flux increases downstream with most of that flux derived from watershed processes outside of Y-12. Previous research indicates that in-stream processes, as opposed to out-of-stream processes, control net MeHg concentration (Riscassi et al. 2016). These baseflow estimates provide valuable insight into contributing and controlling processes in the watershed; however, most of the material flux occurs under stormflow conditions (Riscassi et al. 2016). Our ability to calculate storm flow fluxes along EFPC have been hampered by incomplete and inaccurate rating curves.

Rating Curve Development

Rating curves are empirical equations that relate water level in the stream to volumetric water discharge. Combined with concentration measurements, the discharge estimates enable the calculation of material flux. Rating curves are not static relationships—they depend on channel geometry, which changes with bed scour and deposition events that occur with flooding, bank erosion, and active stream management. Therefore, rating curves need to be verified and remeasured frequently. Additionally, accurate rating curves are developed by making measurements over a broad range of flow conditions to capture both base flow and storm flow. For a stream the size of EFPC, base flow discharge can be made with wading measurements—physically standing in the stream with instruments to make the measurements. However, even in EFPC, wading measurements are not safe under storm flow conditions.

Undiagnosed errors in rating curves for EFPC that date back to the early 1980s resulted in upstream flood discharge estimates being much greater than downstream discharge estimates. Consequently, water and material balances and fluxes that depend on those discharge estimates were wrong. This then leads to incorrect source attribution and misunderstanding of essential components of watershed behavior. To address this knowledge gap and enable future studies of material flux, we acquired an acoustic Doppler current profiler (ADCP; SON-TEK River Surveyor M9) to measure creek discharge across a broad range of flow conditions (Figure 10). The ADCP is a float-mounted, Bluetooth, and GPS-enabled instrument that applies the Doppler principle to measure water velocity at high spatial resolution. Importantly, the ADCP is a non-wading instrument, so personnel can remain safely on shore to make measurements under extreme flow conditions.

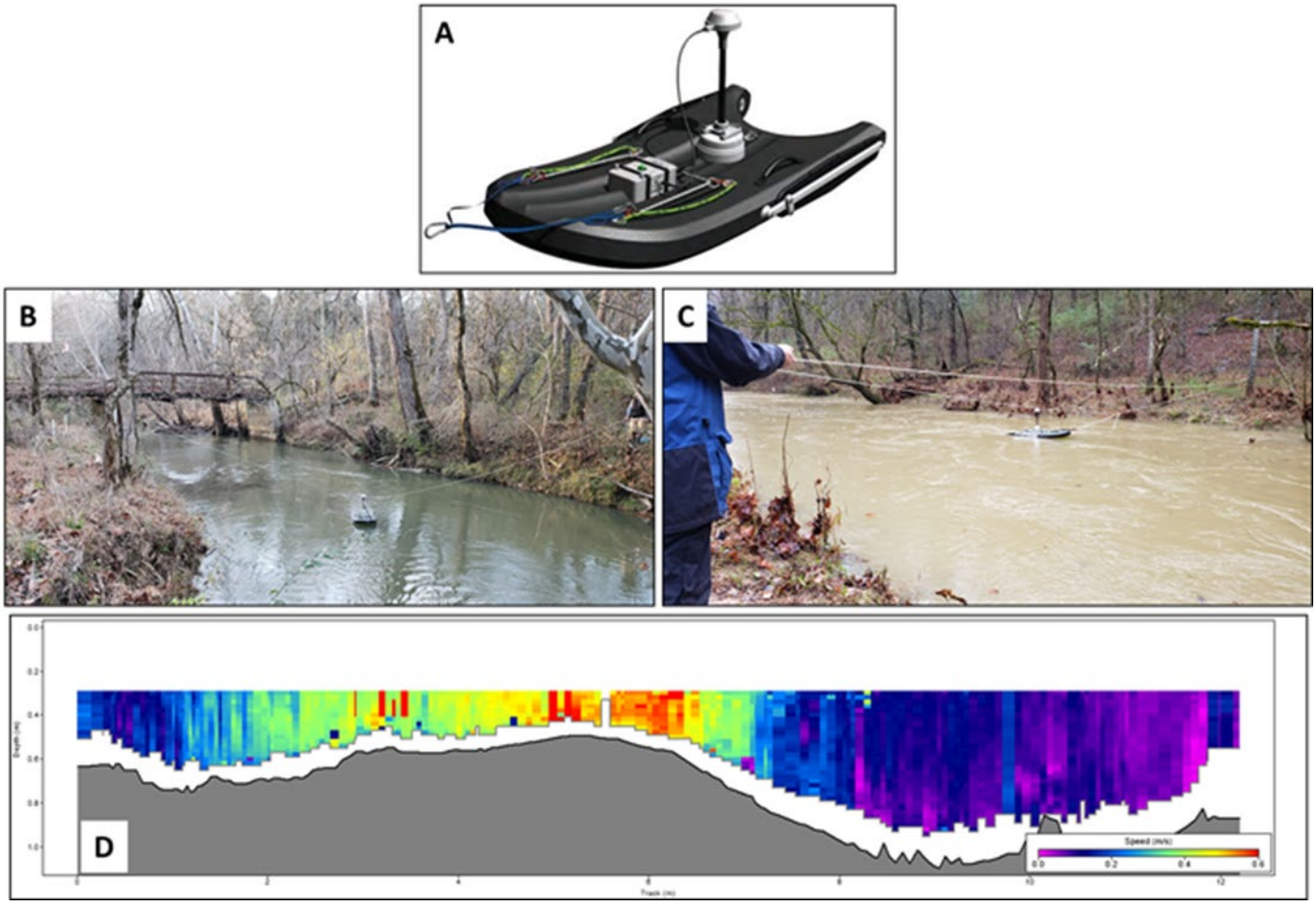

Figure 10. (A) The SON-TEK River Surveyor M9 ADCP showing float, power supply, and GPS antenna. The acoustic sources and receivers are on the bottom of the float. Making discharge measurements with the ADCP under (B) base flow and (C) flood conditions. The water depth in (C) is over 8 ft with mean stream velocity of 3 ft/s and staff can still collect data safely. (D) Stream velocity cross section collected with the ADCP illustrating the lateral and vertical resolution obtained.

Using the ADCP instrument, we are developing new rating curves at our two monitoring stations at EFK 16.2 (Wiltshire Drive) and 5.4 (east of the Horizon Center). Initial results have been quite good, and we no longer face the situation in which upstream discharge exceeds downstream discharge under flood conditions (Figure 11). With these updated rating curves, we can plan to monitor the same flood event at multiple locations along EFPC to improve our understanding of material flux, sources, and watershed behavior. Additionally, these improved discharge measurements directly support the watershed modeling efforts in Task 4.

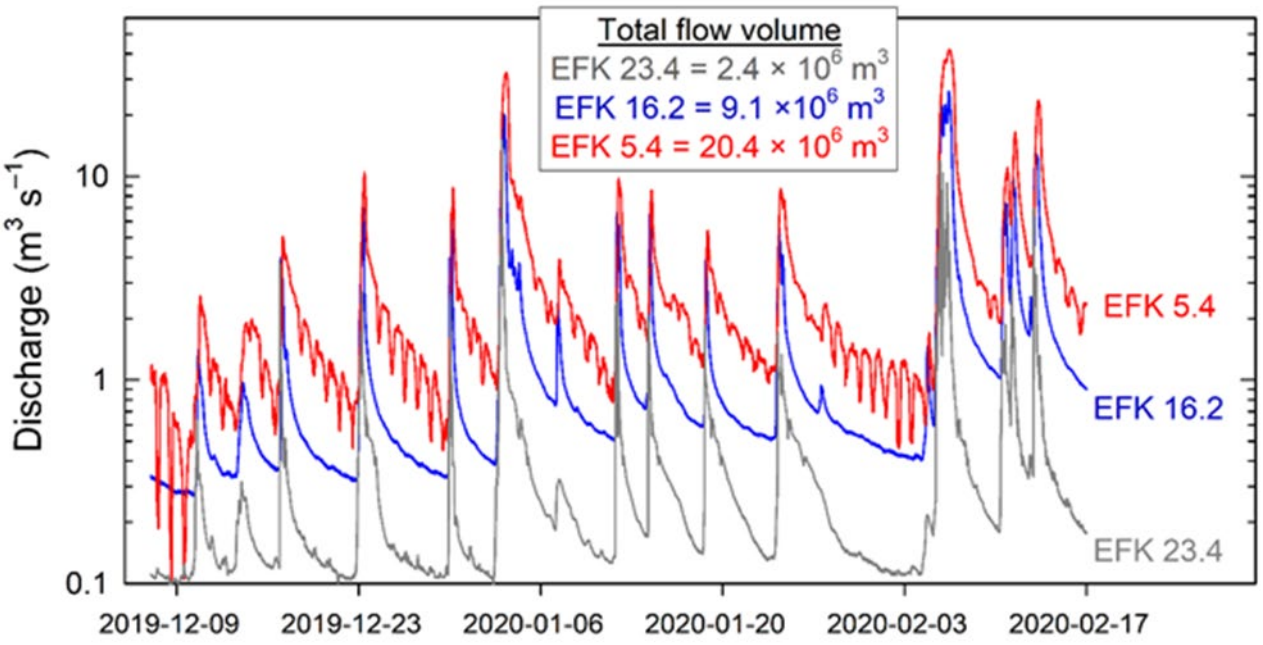

Figure 11. Partial discharge record at three locations along EFPC. Total discharge increases from upstream-to-downstream EFK 23.4, EFK 16.2, and EFK 5.4, reconciling a discrepancy that dates to the mid-1980s.

Sediment Amendments to Decrease MeHg Concentration

MeHg is not a direct contaminant to EFPC but is formed by anaerobic microorganisms in anoxic locations within the creek (e.g., sediments, periphyton biofilms). Previous efforts within Task 2 have evaluated whether engineered sorbents used to remove inorganic Hg from solution would decrease MeHg production (Muller et al. 2019a), and quantified MeHg sorption onto the same sorbents (Muller et al. 2019b). The sorbents tested were effective at decreasing inorganic Hg concentrations in water (Johs et al. 2019) but had no discernible effect on total MeHg production. The sorbents were effective at removing MeHg from solution, but the question remains whether the sorbents will decrease MeHg bioaccumulation (see Future Needs: Surface Water and Sediment).

Sorbent-mediated decreases in water concentration of MeHg is encouraging even if total MeHg concentration is unaffected. Nevertheless, we seek sediment amendments that can decrease total MeHg concentration (water + sediment) by decreasing the production of MeHg, enhancing MeHg demthylation, or a combination of both processes. Over the past several decades, a small number of studies have reported lower MeHg concentration when manganese (Mn) oxides or Mn oxide–coated clays are added to sediment microcosm incubations. For example, Jackson (1989) reported lower MeHg concentration when manganite-coated clay colloids were added to incubations. The results were varied significantly and depended on the addition of dissolved organic matter (DOM), other nutrients, and total Mn. In some cases, more MeHg was produced. In light of the variability, unifying conclusions were elusive, and the author speculated on a combination of effects ranging from direct effects on microbial metabolism to abiotic demethylation. Farrell et al. (1998), working with pure cultures in the laboratory, reported no net MeHg production when cultures were incubated with birnessite (δ-MnO_2). Again, the authors did not identify a mechanism behind their observation and speculated on several causes, including abiotic demethylation and that sorbed Hg was not methylated. More recently, Vlassopoulos et al. (2018) documented lower water concentrations of MeHg in laboratory mesocosms when sediments were amended with either birnessite or pyrolusite (β-MnO_2). Based on a number of ancillary measurements, these authors concluded that the most plausible explanation for their results was redox poising—the Mn(IV) oxides poised the redox status of the sediments at a value too high for the anaerobic methylating microbes to be active.

These previous literature reports are both encouraging and puzzling. They are encouraging because the observation of lower MeHg concentration in the presence of Mn oxides is a consistent finding. They are puzzling because of the variability in results, the apparent heavy dependence on the system geochemistry, and an incomplete understanding of the

whole system. Each of these studies focused on water concentrations, so there is no data to evaluate if total MeHg concentration was affected.

We conducted initial studies on the fate of MeHg in the presence of an amorphous Mn(IV) oxide ($MnO_{2,am}$) (Murphy et al., in review). Bacteria were intentionally excluded from these experiments so that we could focus on the MeHg-$MnO_{2,am}$ interaction. Additionally, we placed an emphasis on closing the MeHg mass balance in experiments to better determine if any abiotic demethylation occurred. We soon discovered that the $MnO_{2,am}$ created severe analytical problems that decreased MeHg recovery in experiments. This finding alone created questions about previous studies. Once the analytical problems were identified and addressed, we recovered 104% ± 5% of the added MeHg from the experimental treatments and 100% ± 3% from controls (i.e., we found no evidence for abiotic demethylation indicating that loss of MeHg from solution was due to sorption alone). Subsequent experiments quantified MeHg sorption onto the $MnO_{2,am}$ as a function of ionic strength, DOC concentration, and initial MeHg concentration (i.e., sorption isotherms; Figure 12). Similar to our previous studies on inorganic Hg and MeHg, we found that DOM played a controlling role in MeHg sorption onto $MnO_{2,am}$ and that the $MnO_{2,am}$ used in these experiments sorbed much less MeHg than the sorbents we tested previously. Although not explicitly addressed in this work, our results suggest that Mn oxide amendments have direct or indirect effects on methylating microorganisms decreasing total production of MeHg.

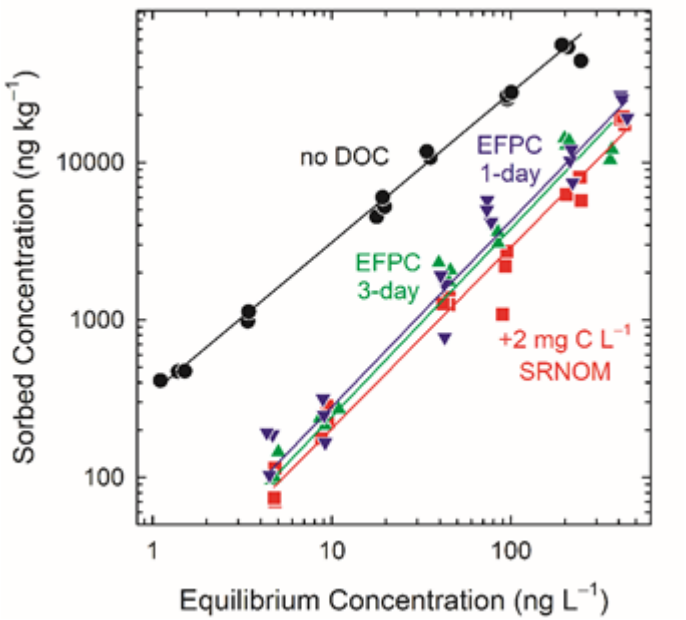

Figure 12. Methylmercury sorption isotherms onto $MnO_{2,am}$ in the absence of DOC, in the presence of 2 mg-C L^{-1} Suwanee River Natural Organic Matter (SRNOM), and in EFPC water equilibrated for either one or three days. EFPC surface water typically contains ~2 mg-C L^{-1} DOC.

Manganese oxides are among the most powerful naturally occurring oxidants. They comprise a broad range of Mn(II/III/IV) oxides in single and mixed Mn oxidation states that span a range of reactivity. Although our initial test with an amorphous Mn(IV) oxide showed no indication of abiotic demethylation, other Mn oxides could catalyze demethylation under similar or different conditions (e.g., pH, incubation length, solid:solution ratio). Further work is being planned to quantify interactions between MeHg and Mn oxides (see Future Needs: Surface Water and Sediment).

Changes to Water Quality Following Termination of Flow Management

Stream restoration activities in EFPC have included the initiation of a flow management program in 1996 to restore minimum baseflow in the uppermost reaches of the creek by pumping in uncontaminated water from Melton Hill Lake.

This water constituted ~8.5% of the mean daily flow measured at a point 21 km downstream and delivered substantial loads of DOC (~25 kg d^{-1}) and total suspended solids (166 kg d^{-1}). The flow management program was halted at the end of April 2014. We conducted regular water sampling for two years along the length of EFPC during the flow management program and five years after flow management was stopped. Most water quality parameters, including DOC concentration, remained unchanged after flow management stopped. Nevertheless, $SUVA_{254}$, a measure of DOM composition, increased suggesting a change to DOM with higher molecular weight and aromaticity. $SUVA_{254}$ has been positively correlated with dissolved Hg concentration, the rate of dissolution of Hg sulfide minerals, and Hg methylation potential (Dittman et al. 2009; Waples et al. 2005; Graham et al. 2013).

In EFPC, the increasing $SUVA_{254}$ coincided with increasing dissolved Hg concentration and decreasing Hg solid-water partitioning coefficients throughout EFPC. Higher $SUVA_{254}$ and dissolved Hg concentration have potential implications for bioavailability and MeHg production. Total and dissolved MeHg concentrations have increased in EFPC since the end of the flow management program and these increases are most pronounced during spring and early summer when biota are more susceptible to exposure and uptake (Riva-Murray et al. 2013) (Figure 13). Similar MeHg concentrations have not been seen in 20 years and in some locations are the highest on record. Other watershed-scale factors likely contribute to the observed patterns as these changes occurred over months rather than instantaneously after flow management stopped and coincided with a general warming trend in the creek. Nevertheless, similar changes in MeHg have not been observed in Mill Branch, a tributary to EFPC.

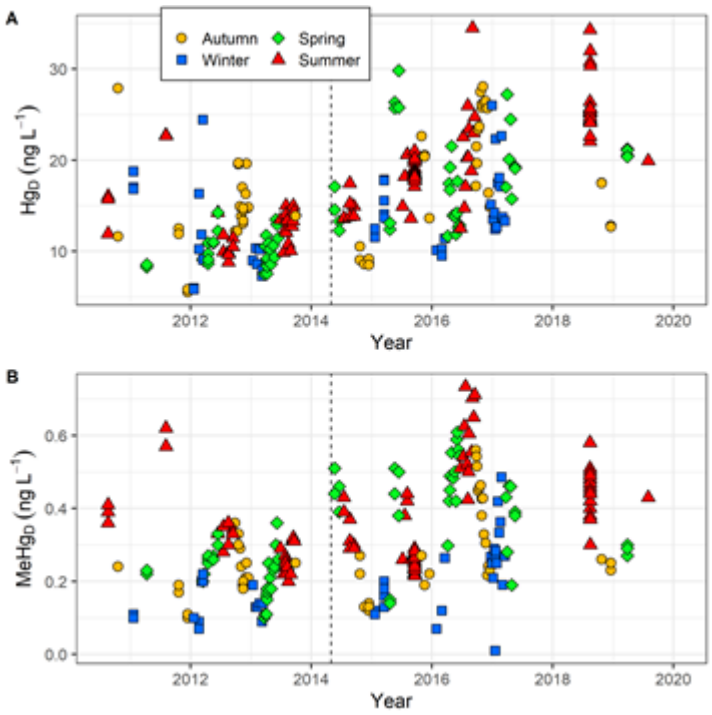

Figure 13. (A) Dissolved total Hg (Hg_D) and (B) dissolved MeHg ($MeHg_D$) concentrations over time at EFK 5–9.5. The vertical dashed line in each plot marks the end of the flow management program.

Future Needs: Surface Water and Sediment

Within this task are several areas of continuing and new research that are warranted. Ambient water quality and flow data have supported new information on Hg and MeHg concentration, flux, and possible sources in the LEFPC watershed. Based on mass balance calculations, we identified the upper reach of the study area as a source of legacy Hg loading to the creek. The dominant source of that Hg is likely the documented HRD deposits. Perhaps equally important and less well understood are the locations, sources, and controls on intermittent Hg loading in the lower study reach. Additionally, there have been significant trends of increasing Hg and MeHg flux at both downstream monitoring points, demonstrating the dynamic changes that occur in the system without direct engineered intervention. Continued monitoring will strengthen the BL record of flux and concentration against which system responses to natural forcings, directed actions (e.g., MTF construction, bank stabilization), and unintentional events (e.g., spill and leaks) can be compared.

Material Flux under Stormflow Conditions. Our previous mass-balance based flux estimates have been limited to base flow conditions because of incomplete rating curves at our monitoring stations. However, we now have updated rating curves that will support monitoring storm driven high-flow events at multiple locations to quantify Hg and MeHg flux along EFPC. Current planning is underway to coordinate and stage in preparation for sampling future storm events. These storm sampling studies will provide data on total Hg and MeHg flux and dynamics during storm-driven flood events that provide insight into material sources, sinks, and watershed function.

Sediment Amendments to Decrease MeHg Concentration. We will continue our study of MeHg removal from the system using sediment amendments. One aspect of this work includes further evaluation of the fate of MeHg in the presence of Mn oxides. In addition to providing needed information for possible water treatment approaches, the MeHg-sorbent work provides a basis for understanding another phase of our planned work. A critical knowledge gap is whether sediment amendments affect bioaccumulation when sediment-sorbent mixtures are ingested by biota at the bottom of the food web. If amendments can decrease MeHg uptake by biota at the lowest levels of the food web, where the greatest biomagnification values are frequently observed, this benefit should propagate up trophic levels, ultimately resulting in lower MeHg concentrations in fish. We are planning a series of tests using water and sediments from EFPC in which we will test the ability of amendments to decrease MeHg concentration in benthic invertebrates. This effect may be due to effective sorption of MeHg as in the case of sorbents we have tested, or lower MeHg production as may be the case for Mn oxide–based amendments. Finally, we are in negotiations with Albemarle Corporation to obtain some of its

developmental and proprietary sediment amendment for Hg treatment that will be incorporated into our studies. These studies will rely on capabilities made available through the AEL upgrade.

Nutrient Effects on MeHg Concentration. Finally, EFPC has a very high nutrient load and is mesotrophic to eutrophic along its length with respect to both nitrogen and phosphorous because of point source and diffuse discharges to the creek. Previous studies of the microbial communities in EFPC suggest lower diversity and richness relative to reference streams. Other measures of EFPC functions suggest the system is stressed. Nutrient uptake velocity is a measure of biotic demand relative to concentration and relates to nutrient retention efficiency. Uptake velocity normalizes for the effects of discharge and stream width, allowing comparison among streams of different sizes. High uptake velocities are consistent with high biotic demand and nutrient use efficiency, whereas low values suggest low biotic demand and reflect ecosystem stress. We calculated nitrate uptake velocity for the upper and lower sections of EFPC where the creek is second order and third order, respectively, and compared those values with other streams, including those that did and did not have point source nutrient inputs. EFPC had very low nitrate uptake velocities (~0.1 mm/min) compared with all streams and compared with streams of the same order (ranging from ~1 to 10 mm/min). Additionally, uptake velocities were low with respect to other streams having point source nutrient inputs. We are planning a series of experiments to test the effect of lowering these high nutrient levels on MeHg production in simulated creek environments. These studies will rely heavily on the use of the renovated stream mesocosms that will be part of the AEL upgrade.

Ecological Manipulation

Role of Ecology in EFPC

The primary goal of ecological manipulation in EFPC is to examine strategies to reduce Hg bioaccumulation in fish in EFPC through sustainable biological or ecological manipulations. In contrast to virtually all other metals, Hg (especially in its organic form, MeHg) biomagnifies or becomes increasingly concentrated as it is transferred through aquatic food chains to higher trophic levels, namely to fish. Consequently, the consumption of Hg-contaminated fish is the primary exposure route to humans. For this reason, the National Recommended Water Quality Criterion (NRWQC) for Hg is based on a fish tissue concentration rather than an aqueous Hg concentration because the tissue concentration (0.3 mg/kg) is considered to be a more consistent indicator of exposure and risk to humans and aquatic life.

Although most Hg in the environment is inorganic mercury (Hgi), a small proportion of total mercury (Hg_T) is microbially transformed to MeHg in the aquatic ecosystem. Anoxic reducing environments such as wetlands are considered Hg-methylating hot spots, where large amounts of Hgi are methylated by sulfate- and iron-reducing bacteria. However, recent research has highlighted freshwater streams as sites of Hg methylation, with favorable conditions for methylation including increased temperatures, the presence of certain filamentous algae, and the presence or absence of certain organic nutrients (Tsui et al. 2010). The methylation of Hg from periphyton- and macrophyte-associated bacteria has also highlighted additional opportunities for Hg methylation within freshwater streams (Acha et al. 2012).

Methylmercury readily crosses cell membranes and binds with proteins, forming complexes that mimic essential amino acids. Therefore, MeHg is highly bioaccumulative, becoming incorporated into protein-rich tissues (e.g., muscle; typically, MeHg is >95% of the HgT in fish fillets) with long residence times. In aquatic animals, MeHg uptake rates from water and assimilation efficiencies from food are high, whereas elimination rates are low, leading to progressively increasing concentrations within organisms over time. This also leads to progressive concentrations of Hg within food chains as MeHg transfers from one trophic level to the next.

One of the challenges to effective remediation at Hg-contaminated sites is that while Hg body burdens in fish are often more closely linked to aqueous MeHg than Hgi concentrations (Tom et al. 2010), MeHg production is not easily predicted or controlled. For example, in systems contaminated by atmospheric deposition with low aqueous HgT concentrations (<10 ng/L), a correlation exists between Hg(II) and MeHg concentrations (Kelly et al. 1995). However, in point source contaminated systems, waterborne Hgi concentrations can range over several orders of magnitude, while MeHg concentrations in water and biota seldom differ by more than 10-fold (Southworth et al. 2004). Decreasing aqueous Hgi concentrations and loading might often be a more achievable remediation goal than decreasing MeHg concentrations, but this approach has led to mixed results in terms of responses in fish bioaccumulation. Numerous source control measures

have resulted in rapid responses in lake or reservoir fisheries (Joslin 1994; Turner and Southworth 1999), but examples of similar responses in Hg-contaminated stream ecosystems are less common. Recent work suggests that stream systems might actually be more susceptible than lakes to Hg bioaccumulation, highlighting the need to better understand the ecological drivers of Hg bioaccumulation in stream-dwelling fish (Chasar et al. 2009; Ward et al. 2010). Although Hgi concentrations play a part in determining overall Hg concentrations in fish, methylation efficiencies and food web pathways are also important in determining fish tissue concentrations.

Effective Hg remediation in EFPC requires not only an understanding of the nature and magnitude of Hg inputs but also knowledge of the extent to which these inputs must be controlled to achieve the desired reduction of Hg contamination in biota necessary to meet the NRWQC. However, because Hg is accumulated predominantly through the food chain rather than through aqueous exposure, understanding food web structures and transfer pathways for Hg to fish is a key component to successfully implementing strategies to mitigate Hg bioaccumulation. Uptake at the base of the aquatic food chain (algae/periphyton, invertebrates) is the most important concentration step for Hg (with Hg concentrating more than 10,000-fold between water and algae). However, although the relationship between Hg concentrations in water and fish has been characterized, transfer pathways from the base of the food chain remain largely unknown.

Resolving key questions concerning the role of ecological interactions in driving fish tissue Hg concentrations in EFPC required quantifying Hg and MeHg inventories throughout food webs at various locations throughout EFPC (Peterson et al. 2015). Biological Hg and MeHg inventories serve several purposes for site management and technology development, including (1) supporting conceptual model development and site characterization; (2) assessing exposure and risk evaluation; (3) informing site prioritization; (4) informing remediation selection and design; and (5) providing BL information for performance, compliance, and long-term monitoring and evaluation. The conceptual model for remediation targets in EFPC assumed that Hg accumulation in fish in EFPC was proportional to waterborne HgT. This assumption was the basis for derivation of the aqueous Hg target guiding Comprehensive Environmental Response, Compensation, and Liability Act of 1980 efforts in UEFPC (200 ng/L). Over the past decade, aqueous HgT concentrations in UEFPC have been fluctuating because of various activities (e.g., operation of the Big Spring Water Treatment System, storm drain cleanouts, cessation of flow augmentation, demolition activities), and fish do not appear to be responding to these changes. Lack of a clear response suggests that the relationship between Hgi concentration and the MeHg production/bioaccumulation observed in UEFPC in the 1990s is not a straightforward, linear relationship.

To address these needs and fill knowledge gaps, we sampled biota throughout the food web at four biological monitoring sites in EFPC (EFK 23.4, 18.2, 13.8, and 6.3). We quantified MeHg and total MeHg and estimated trophic status using stable isotopes of carbon and nitrogen to assess the relative importance of food web dynamics in determining Hg bioaccumulation in fish. We examined a food web model to identify the most important factors affecting Hg concentrations in fish, and based on the results, we began laboratory experiments to examine the potential effects of adding native freshwater mussel species to EFPC.

The Role of Mussel Filtration on Hg Dynamics

A statistical examination of the factors influencing Hg concentrations in fish in EFPC showed that, unsurprisingly, aqueous MeHg concentrations significantly and positively correlated with Hg fish tissue concentrations. This examination, which considered 30 years of community structure data in EFPC, also showed that the percentage of collector filterers in the community significantly and negatively correlated to Hg in fish (Figure 14). This finding led to an ongoing investigation of the potential of introducing native freshwater mussels into EFPC to mitigate Hg bioaccumulation in fish.

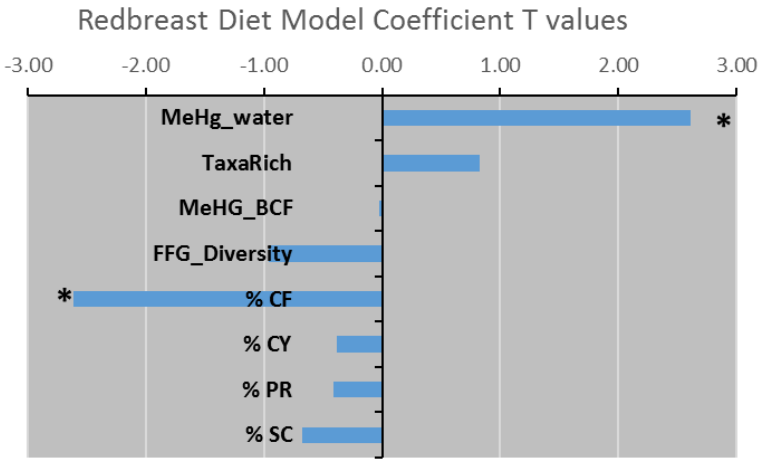

Figure 5. Linear mixed model developed for redbreast diets under different scenarios. The predictor variables for MeHg in the diet were aqueous MeHg, taxa richness, bioconcentration factors (BCFs), functional feeding group (FFG) diversity, percent of collector filterers (CFs) in the invertebrate community, percent crayfish (CY), percent predators (PR), and percent scrapers (SC). Values shown are T value coefficients. Asterisks denote significant values.

Freshwater mussels are filter feeders, filtering large volumes of water over their gills to remove algal and detrital particles for nutrition. Because mussels filter particulates from the water column, they can significantly affect water quality (Figure 15) and, therefore, play a critical role in freshwater ecosystems. These species are of interest in EFPC because they can affect Hg bioaccumulation throughout the food web by exerting effects on periphyton, DOM, methylating bacteria, and aqueous Hg concentrations. ORNL scientists are working closely with the Tennessee Wildlife Resource Agency (TWRA), which has a mission of restoring these native species to Tennessee waters. The reintroduction of native mussels to EFPC could not only mitigate Hg bioaccumulation and risks in this stream but also provide other ecosystem services, including water quality improvement and propagation of sensitive native species.

Figure 6. Demonstration of clam and mussel filtration. All aquaria were initially inoculated with the same algal cell concentration. The aquarium in the middle had Asian clams (Corbicula fluminea), the one on the right had Rainbow (Villosa iris) and young Pocketbook (Lampsilis ovata) mussels, and the one on the left had no bivalves. The photo was taken 2 h after adding algae.

To determine the potential effects of mussel filtration on Hg dynamics in EFPC, (1) filtration or clearance rates of mussels under different environmental conditions, (2) Hg removal rates, and (3) effects of mussel filtration on Hg methylation rates must be determined. In past years, we performed field investigations to quantify Hg bioaccumulation rates and laboratory investigations to quantify filtration rates for different species under different environmental conditions.

Our field deployment results showed that Hg bioaccumulation rates in Asiatic clams (*Corbicula fluminea*) were much higher in the spring than in the winter (Mathews et al. 2019). This suggests a positive effect of water temperature on filtration rates. Most biological and metabolic rates are affected by temperature. Microbial activity is also affected by temperature, and Hg methylation rates (which are controlled by microbes) and concentrations are, therefore, also higher in spring in EFPC than in winter. These results suggest a seasonal component to the efficiency of Hg removal but that filter feeders would be removing Hg at times critical to Hg methylation. Our results also show that unlike fish bioaccumulation patterns, clam bioaccumulation is proportional to aqueous Hg concentrations. A strong spatial pattern exists of higher Hg concentrations upstream where aqueous concentrations are highest and significant decreases with increasing distance downstream.

Field collections of resident *Corbicula* in EFPC show a similar spatial pattern to deployed clams, with the highest Hg_T concentrations at upstream sites within EFPC and decreasing concentrations with distance downstream (Mathews et al. 2019). Unlike fish tissue where Hg is predominantly found as MeHg, clams accumulate high concentrations of Hg_i, with MeHg making up only a small fraction of Hg_T. No difference was observed between concentrations in resident clams

collected in spring and fall, likely because once Hg is assimilated, loss rates are low. The concentrations of total Hg in resident clams in EFPC were comparable to clams that were deployed at these same sites for 4 weeks in the spring, suggesting that rather than being a threshold concentration for these organisms, Hg concentrations are coming to an equilibrium between the aqueous phase and biological tissue.

The clams collected in EFPC are significantly smaller in size (mean wet weight ~2 g) than those collected at reference locations (mean wet weight ~4 g), suggesting either that the age structure of the population in EFPC is significantly different than in reference sites or that the population is stunted.

One of the key tasks for the project will be to determine how many mussels it would take to make a significant difference in aqueous Hg concentrations. The first step to determining this is to quantify uptake, loss, and filtration rates of different species under different environmental conditions. Then, we can also use the estimated filtration capacity of Asian clams currently populating the creek to make decisions going forward.

Quantifying Depuration (Loss) Rates

Mercury biomagnifies because it is readily taken up by tissues, is efficiently assimilated (especially as MeHg), and has low loss rates (especially for MeHg). To estimate steady-state concentrations in biota, quantifying uptake and depuration (or loss) rates is necessary. Last year, we conducted a loss rate experiment in which we collected *Corbicula* from each of the five sites within EFPC and from one control site in Brushy Fork Creek. The clams were brought back to the lab and allowed to depurate for 6 weeks in uncontaminated water from First Creek.

Mercury loss rates were highest in clams that were collected from the upper-most sections of EFPC. This is likely because the clams in the upper-most sections of the creek have the highest Hg concentrations, and a much greater proportion of the Hg in their tissues is Hg_i. At sites further downstream, where MeHg makes up a much greater proportion of the total Hg concentration in tissues, loss rates were much lower (Mathews et al. 2019).

Quantifying Filtration Rates

The exotic Asiatic clam is currently the only bivalve species living in EFPC. To assess filtration capacity and quantity of bivalves, including native species, to remediate Hg in the creek, a series of experiments were performed in the laboratory to assess the effects of biotic and abiotic factors on the filtration rates of native mussels species (*Lampsilis ovata* and *Utterbackia imbecillis*) and Asian clams.

Asiatic clams were collected from Sewee Creek in Meigs County. Paper pondshell mussels (*U. imbecillis)* were collected by TWRA personnel from Sumner Sportsman Club Lake in Portland, Tennessee (36.604280, −86.487226). Pocketbook mussels (*L. ovata*) were cultured in TWRA's Cumberland River Aquatic Center.

Bivalves were brought to the laboratory in a cooler with an air bubbler. No mortality was recorded during transportation. The bivalves were kept in 700 or 450 L tanks supplied with flow-through water from First Creek on the Oak Ridge Reservation in Oak Ridge, Tennessee (water renewal: 50–150 L h^{-1}; ambient temperature: 14°C–28°C; light/dark: 12 h/12 h), and acclimated to the laboratory for at least 4 weeks prior to the experiment. In addition to the supply of food particles coming from the water inlet (~1,000 particles mL^{-1}), bivalves were fed a daily diet of fresh algae: *Chlamydomonas reinhardtii* and *Navicula* sp. (~7×10^7 cells ind^{-1} d^{-1}) using a peristatic pump or medical IV drip bags for continuous feeding.

Effects of light on the filtration of freshwater bivalves *C. fluminea* and *U. imbecillis*

In this experiment, we aimed to determine the filtration rates of the Asian clam (*C. fluminea*) and the poorly studied native species *U. imbecillis* under controlled light conditions. Filtration activity was assessed through the determination of clearance rates of the studied species (i.e., volume of water cleared of suspended particles per unit of time).

Clearance rates of each species were determined following the methods of Riisgård (2001). Individuals of both species were placed in separate clear plastic containers with dechlorinated tap water (100 mL in round punch cups for *C. fluminea*

and 500 mL in Lee's specimen containers for *U. imbecillis*) with aeration. One container was kept with no bivalve and used as a control. Preliminary tests were carried out and confirmed that there was no significant difference in cell concentrations between control containers (without bivalves, n = 3), so we used only one control container for each of the experiments. Bivalves were allowed to acclimate until active filtering was observed (~30 min). After the acclimation period, live algae (*C. reinhardtii*) was spiked to each plastic container to reach the targeted initial concentrations. Subsamples of 1 mL water were taken from each plastic container 5 min after the algae spike and then at 5 to 15 min intervals (based on visual color changes in the plastic containers). The filtration was assessed for up to 1 h. The same sampling procedures were conducted for the experiments in the dark condition where no visual observation was possible. Samples were placed in 1.5 mL tubes with 200 µL of 10% formalin solution and mixed immediately. Analyses of the samples were performed using by flow imaging cytometry (FlowCam Benchtop B3 Model).

The experiments were performed for both species in the dark (0.0 µmol m^{-2} s^{-1}) with the initial cell concentrations of *C. reinhardtii* (2.5 ± 0.2 × 10^5 cells mL^{-1}) and in the light (6.5 ± 0.5 µmol m^{-2} s^{-1}) with the initial cell concentrations of *C. reinhardtii* (4.0 ± 0.2 × 10^5 cells mL^{-1}). The sample sizes, the number of individuals tested per treatment, (n = 7 in dark, 8 in light for *C. fluminea*, and n = 6 in dark, 8 in light for *U. imbecillis*) followed the recommendations from Salerno et al. (2018). Light intensity was measured using a PAR meter (Quantum Flux Apogée). Temperature was maintained at 22°C ± 0.5°C during the experiment.

Cell concentration (cells mL^{-1}) kinetics were fitted with an exponential model and linearized by log transformation. Only regressions with $R^2 \geq 0.85$ were considered for clearance rate calculations (Hansen et al. 2011). Clearance rates (expressed as mL g^{-1} h^{-1}) were calculated according to Mistry and Ackerman (2018).

We found that *C. fluminea* filtered significantly faster (110 ± 15 mL g^{-1} h^{-1}, n = 7) than *U. imbecillis* (24 ± 6 mL g^{-1} h^{-1}, n = 6) in the dark condition (Hills et al. 2019). During light conditions, no significant difference was found in clearance rates in *C. fluminea* and *U. imbecillis*, although the average clearance rates were slightly higher in the *C. fluminea* (50 ± 18 mL g^{-1} h^{-1}, n = 8) than those in the *U. imbecillis* (41 ± 10 mL g^{-1} h^{-1}, n = 8) (Figure 16). This noticeable difference of clearance rates in the dark was also revealed in the filtration kinetics of the two species (Figure 17). This finding suggests that the filtration rates of the invasive species *C. fluminea* may be advantageous at night compared with native species.

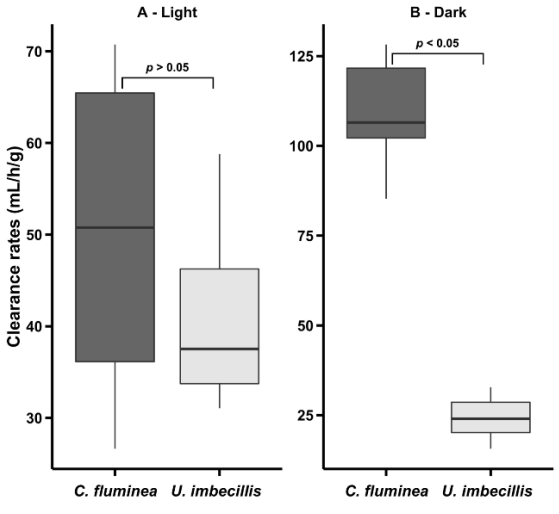

Figure 16. Clearance rates assessed for the two tested species (the Asian clam [C. fluminea] in dark gray and the paper pondshell [U. imbecillis] in light gray) under two light intensity conditions: (A) lightand (B) dark. Whiskers indicate the minimum and maximum values, black lines indicate the median, and boxes represent the 25th and 75th percentile.

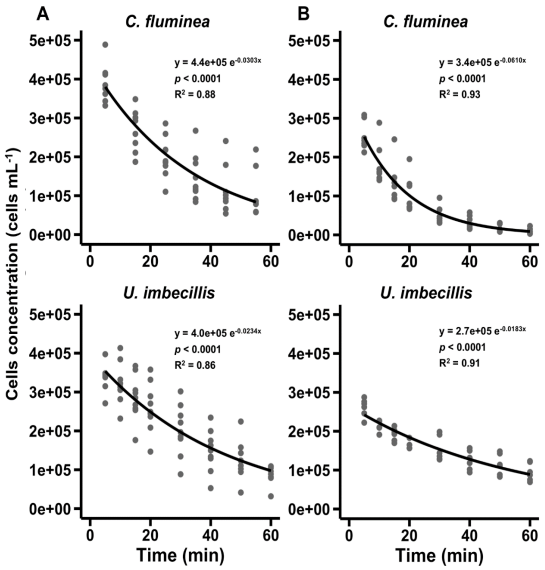

Figure 17. Combined kinetics of all filtration rates for the two tested species, C. fluminea and U. imbecillis, under two light conditions: (A) light and (B) dark.

These results provide preliminary insights to the potential for species competition if both were to exist in EFPC simultaneously.

Combined effects of food, light, and temperature

Effects of light and temperature on the clearance rates (i.e., volume of water cleared of suspended particles per unit of time) (Riisgård 2001) of two bivalve species—the Asian clam (*C. fluminea*) and the pocketbook mussel (*L. ovata*)—were assessed under controlled laboratory conditions at two concentrations of algal food: "low" food (i.e., 10,000 cells mL^{-1}) and "high" food (i.e., 100,000 cells mL^{-1}). Using the collected data from the two experiments, the relative contribution of each tested variable (i.e., food, temperature, and light) on the clearance rate of each species was assessed (Pouil et al., in review).

To assess the effects of food concentration on clearance rates of *C. fluminea* and *L. ovata*, two experiments were performed in the same temperature (10°C, 15°C, 20°C, and 25°C) and light (19 ± 2 µmol m^{-2} s^{-1} and 0 ± 0 µmol m^{-2} s^{-1}) conditions (Figure 18). In Experiment 1, bivalves were acclimated to temperature and food ration (1.2×10^7 cells ind^{-1} d^{-1}), and then clearance rates were assessed using *C. reinhardtii* at a concentration of 10,000 cells mL-1 (i.e., low food condition). In Experiment 2, after an additional week of acclimation to a 10-fold increase of the food ration (12×10^7 cells ind^{-1} d^{-1}), clearance rates were assessed at the second *C. reinhardtii* concentration (i.e., 100,000 cells mL^{-1}, high food condition).

In each experiment, eight individuals of each bivalve species were randomly selected for each experimental temperature (*C. fluminea*: 2.06 ± 0.35 g wet wt, 16.9 ± 0.8 mm shell length; *L. ovata*: 0.54 ± 0.13 g wet wt, 16.4 ± 1.2 mm shell length). On the day of the experiment, each individual was weighed and placed in a food-grade PET container filled with 200 mL of stream water. The temperature was kept constant in the containers at targeted experimental treatments by using chilled or heated water baths. Three containers per temperature treatment were used as controls with no bivalve. Slight air bubbling in each container kept water well circulated. Bivalves were acclimated to experimental containers for 4 h. The sample sizes (n = 8 per temperature for each species) followed the recommendations from Salerno et al. (2018). At the start of the experiment, concentrated live *C. reinhardtii* cells were spiked into each plastic container to add the targeted initial concentration. A 4 mL sample was taken from each plastic container 5 min after the algae spike and then a second 4 mL sample at the end of the 35 min filtration period. Samples were placed in -mL snap-cap centrifuge tubes containing 800 µL of 10% formalin solution, a common preservative for phytoplankton samples (Mukherjee et al. 2014), and mixed immediately. Analyses of the samples were performed using flow imaging cytometry (FlowCam Benchtop B3 Model). In a single day, each experiment was first performed in light conditions (i.e., at 2 p.m.: 19 ± 2 µmol m^{-2} s^{-1}). Each PET container was cleaned and rinsed with dechlorinated tap water, refilled with stream water at the appropriate temperature, and the same organisms were acclimated for another 4 h. The same experiment was then repeated in dark conditions (i.e., at 8 p.m.: 0 ± 0 µmol m^{-2} s^{-1}).

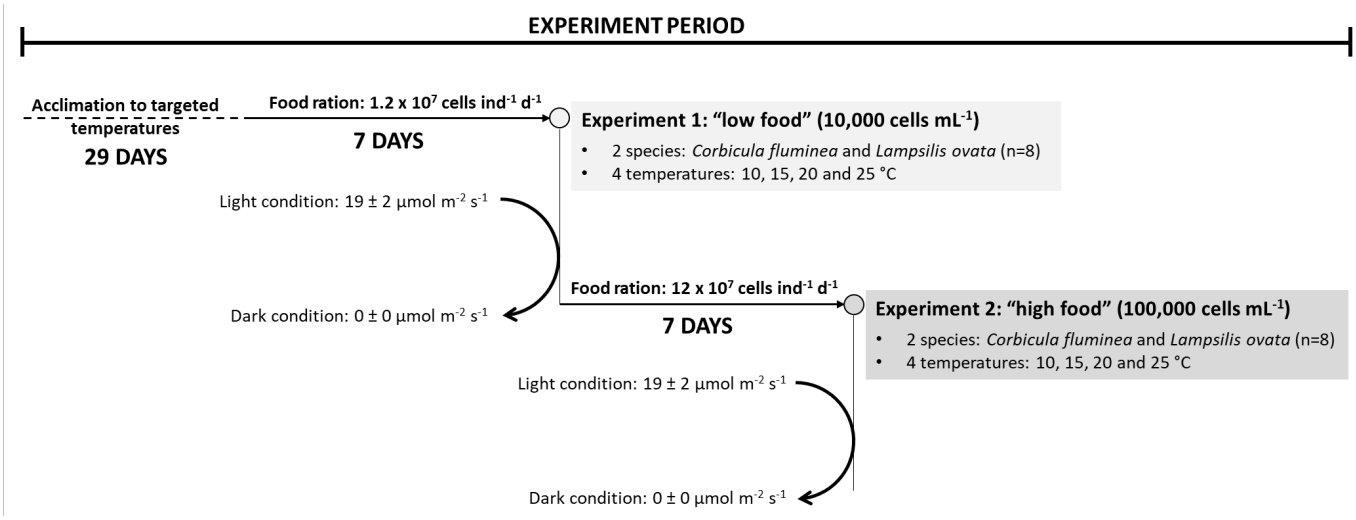

Figure 18. Diagram of the protocol used to test effects of temperatures on the clearance rates of C. fluminea and L. ovata. Experiments were repeated the same day using the same individuals at the two light intensities, first at the low concentration of food and then one week later at the high concentration of food after acclimation to a 10-fold higher food daily ration.

In the low food concentration experiment, after combining all the temperature and light conditions, clearance rates ranged from 0 to 472 mL g^{-1} h^{-1} (median value: 186 mL g^{-1} h^{-1}) for *C. fluminea* (n = 64) whereas the median clearance rate of *L. ovat*a (n = 64) was 2.5-fold higher (i.e., 455 mL g^{-1} h^{-1}) and values ranged from 0 to 905 mL g^{-1} h^{-1} (Figure 19A). Interestingly, the proportion of individuals filtering during this experiment also differed according to species. While most of the *L. ovata* were filtering regardless of the temperature and light conditions (88%–100% of individuals filtering), the proportion of individuals filtering was more variable for *C. fluminea*: in both light and dark conditions, 100% of the individuals were filtering at 15°C , but only 88% at 10°C and 20°C and 75% at 25°C (Figure 19B).

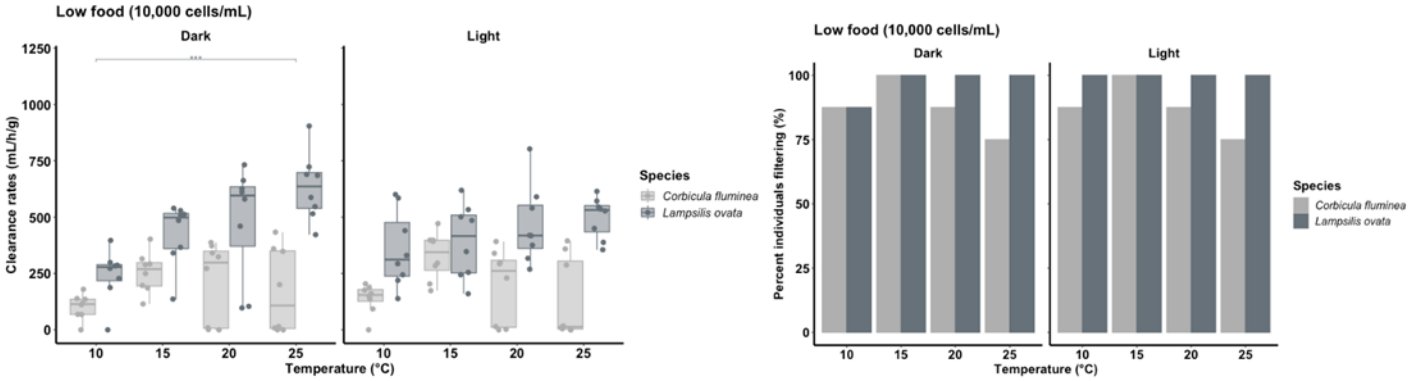

A B

Figure 19. (A) Effects of temperatures on the clearance rates of C. fluminea and L. *ovata exposed to the two light intensities and the low concentration of food. Symbols denote significant differences. (B) Percentage of individuals filtering during this experiment.*

A three-way mixed analysis of variance was performed to evaluate the effects of temperature and light on clearance rates of two bivalve species. The three-way interaction among temperature, light, and species was not significant, but a statistically significant simple two-way interaction was found between temperature and species, indicating that effects of temperature is species-dependent. Thus, although significant effects of temperature on clearance rates of *L. ovata* in the dark were not observed, no statistical difference was observed for *C. fluminea* maintained in the same light condition. For both species, no significant effect of temperature was found in the light condition. Pairwise comparisons tests revealed that for *L. ovata* in the dark, clearance rates were significantly different between 10°C and 25°C. No significant difference was observed for other temperatures (Figure 20).

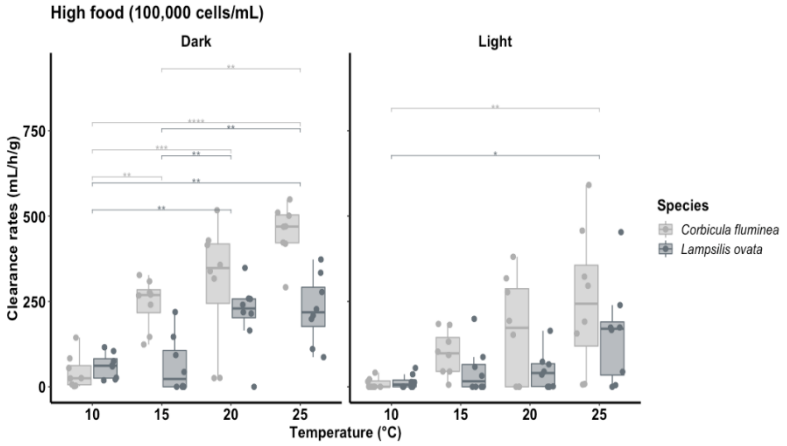

A

The second experiment was performed after one week of acclimation to a 10-fold higher daily food ration to assess clearance rate at the high concentration of food (i.e., 100,000 cells mL^{-1}). When all temperature and light conditions were combined, the clearance rates ranged from 0 to 591 mL g^{-1} h^{-1} (median value: 154 mL g^{-1} h^{-1}) for *C. fluminea* (n = 64) and 0 to 453 mL g^{-1} h^{-1} (median value: 62 mL g^{-1} h^{-1}) for *L. ovata* (n = 64, Figure 20A). While median values were similar at the two food concentrations in *C. fluminea*, median values for the *L. ovata* clearance rate was more than 7-fold higher at the high food concentration than the one observed at the low food concentration. The proportion of individuals filtering also differed between the two experiments. In the high food condition, in the dark, all the *C. fluminea* were filtering in all temperatures. For the same species, filtration activity highly depended on temperature and light conditions (38% at 10°C vs. 100% at 15°C and 25°C). For *L. ovata*, in the dark, all the individuals were filtering at the extreme temperatures (i.e., 10°C and 25°C) whereas this proportion decreased to 88% at 20°C and 63% at 15°C. The proportion of *L. ovata* individuals filtering in light increased with increasing temperatures from 50% at 10°C and 15°C to 88% at 25°C (Figure 20B).

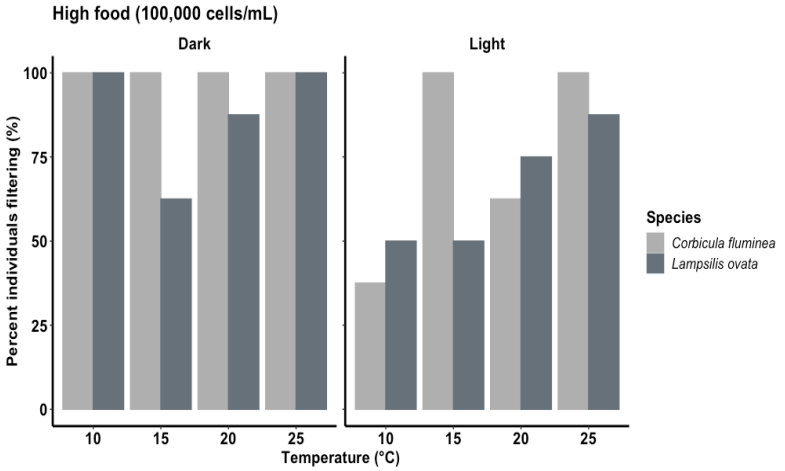

Figure 20. (A) Effects of temperatures on the clearance rates of C. fluminea and L. ovata exposed to the two light intensities and the high concentration of food. Symbols denote significant differences. (B) Percentage of individuals filtering during this experiment.

Similar to the low food concentration tested, the three-way mixed analysis of variance for the high food concentration revealed that interaction between temperature, light, and species was not significant. However, the two-way interaction between temperature and species was significant. Significant effects of temperature were observed on clearance rates of *C. fluminea* in the dark and in the light. Significant effects were also found for *L. ovata* in the dark and in the light. In the dark condition, clearance rates gradually increased with the increasing temperatures for the two species. In the light condition, clearance rates of the two species were only significantly different between the extreme temperatures tested (i.e., 10°C and 25°C, Figure 20).

To summarize the overall effects of food, temperature, and light on clearance rates, GLM models were implemented. For *C. fluminea*, temperature and to a lesser extent light played a significant role in clearance rate, whereas clearance rate was not affected by the 10-fold difference in food concentration applied in the experiments performed. Interestingly, for *C. fluminea*, only 16% of the variance observed in clearance rates was explained by the model. Temperature had the highest contribution (80%, CI: 64%–98%) while light had a moderate effect and food had virtually no effect on the clearance rate (19%, CI: 2%–28% and 0%, CI: 0%–9%, respectively). For *L. ovata*, the clearance rate was significantly affected by food, temperature, and light, with a high proportion of the observed variance explained by these three variables (67%). Among these, food clearly had the highest contribution (81%, CI: 72%–89%) while temperature and light had moderate effects on the clearance rate (18%, CI: 11%–22% and 2%, CI: 0%–6%, respectively; Figure 21).

The effect of environmental factors on each species can vary greatly. These results further support the need for future experiments on additional species.

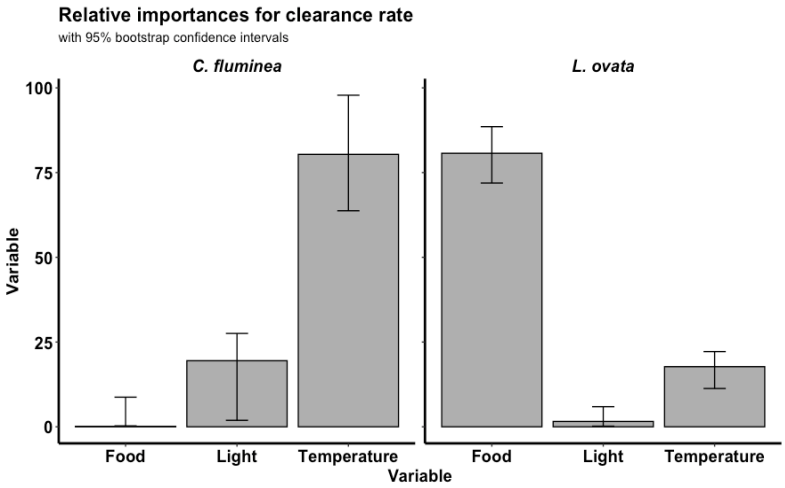

Figure 21. Relative contribution of each explanatory variable (i.e., food, temperature, and light) on the clearance rates of each species: C. fluminea and L. ovata. Values are means with 95% bootstrap confidence intervals.

Modeling the Filtration Capacity of Bivalves in EFPC

The laboratory work to estimate filtration rates and Hg uptake and loss rates will ultimately be used to estimate the potential effects of mussel filtration on Hg dynamics in EFPC. Last year, we used laboratory-derived parameters (e.g., filtration rates), field variables related to habitat (e.g., flow regime, substrate, canopy), and a *Corbicula* population estimation to provide a preliminary estimate of filtration capacity of the existing clam population in EFPC. We estimated total clam mass in EFPC to be 30,996.655 kg (prediction interval: 2,080.819–365,516.734 kg). We estimate current total *Corbicula* filtration capacity in EFPC to be [0.102 $L \cdot hr^{-1} \cdot g^{-1}$ × 30,996,655.0 g] = 3,161,658.8 $L \cdot hr^{-1}$, with a prediction interval range of 212,243.5–37,282,706.9 $L \cdot hr^{-1}$. The mean filtration capacity per square meter of stream bottom is 13.30 $L \cdot hr^{-1} \cdot m^{-2}$, with a range of 0.8927 to 156.8 $L \cdot hr^{-1} \cdot m^{-2}$ (Mathews et al. 2019).

To increase model accuracy, we had planned to sample additional sites in summer 2020. However, because of pandemic-limited personnel on campus, this has been postponed.

Laboratory experiments on the filtration rate of *C. fluminea* performed during this fiscal year (detailed above) allowed us to assess the influence of some major abiotic and biotic factors affecting bivalve populations and, more generally, stream ecosystems: temperature, light, and food availability. Thus, these laboratory data will enable refining the estimated filtration capacity of the existing clam population in EFPC. However, because size is known to affect the filtration rate in bivalves, an experiment is currently set up in the laboratory to investigate filtration rate of *C. fluminea* (n = 150) of a wide size range (from <1 to >10 g whole body weight).

Mercury Toxicity in Aquatic Invertebrates

After the experiments outlined above, we will have data on Hg uptake and loss in Asian clams, as well as filtration rates. The next steps will be to collect similar data on freshwater mussels. We have some filtration rate data on some species of native mussels, but we have not exposed any of them to Hg yet. This is a key part of estimating the number of mussels required to naturally remediate some Hg from EFPC. Therefore, we have performed toxicity tests to assess the effects of Hg on a model aquatic invertebrate: *Ceriodaphnia dubia*. In this species, we looked at the effect of Hg on survival, reproduction, and growth (Figure 22). Such data are useful to provide a BL of Hg sensitivity to invertebrates and, thus, further assess the effects of mitigation strategies, including the use of SnCl (Mathews et al. 2015).

Figure 22. Mercury toxicity test (example) with Ceriodaphnia dubia for preliminary BL data for future mussel work.

Toxicity of different concentrations of Hg (500, 500, 10,000, 17,500, and 25,000 ng L^{-1}) was investigated in a chronic toxicity test. A treatment of DMW25% EDTA-free synthetic freshwater media was used as a control. The test was carried out according to US Environmental Protection Agency guidelines. Briefly, 15 neonates from laboratory cultures and born in the same 8 h period the day before the experiment were used per condition. Each neonate was transferred in a 20 mL

borosilicate vial filled with DMW25% EDTA-free media with the appropriate concentrations of Hg. All the neonates were kept in an incubator set at 25°C with 16 h of light (10–20 µmol m^{-2} s^{-1}).

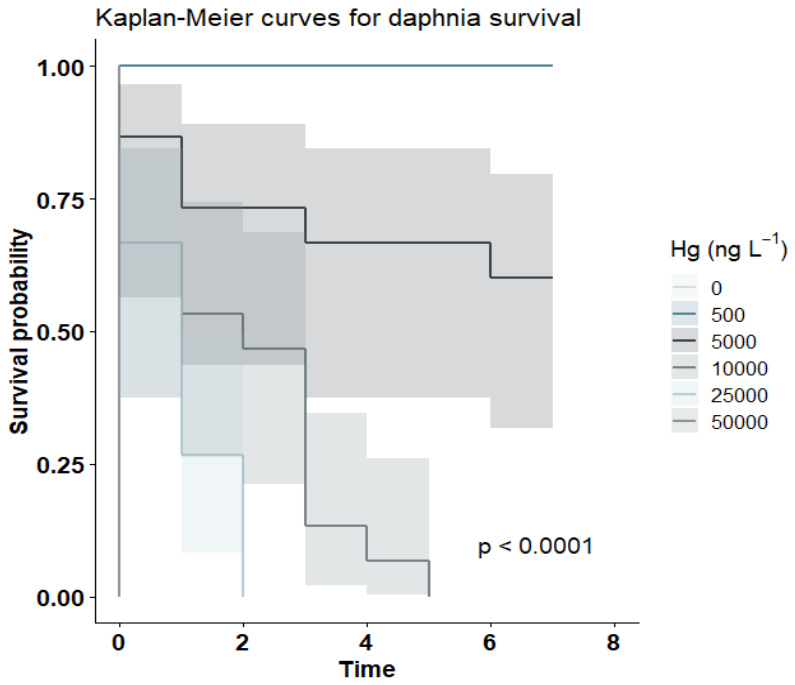

Figure 23. Survival probability of Ceriodaphnia dubia exposed to a gradient of dissolved Hg concentrations estimated through a Kaplan-Meier analysis.

Every day during the 7-day experiment, media for the different conditions were prepared and Hg concentrations were checked by Cold Vapor-Atomic Absorption. The treatment water was then changed in all the experimental vials, and neonates were transferred into the freshly prepared vials and fed with 3 × 10^6 cells ind^{-1} of *Pseudokirchneriella subcapitata* (ex *Raphidocelis subcapitata*) and 100 µL of yeast. Survival and reproduction were followed every day during the transfer of each daphnid. Water quality (pH, conductivity, O_2) of the DMW25% media was checked every day before and after exposure.

Growth, estimated by measuring the length of the daphnia from the top of the eye to the base of the spine according to Agatz et al. (2015), was checked every two days during the experiment using a stereomicroscope (Leica M80), which was calibrated using a 200 µm stage micrometer.

Survival through time was significantly affected by the Hg exposure concentrations (Figure 23). Indeed, while in the control condition (Hg: 0 ng L^{-1}) and at the lowest Hg concentration (i.e., 500 ng L^{-1}), no mortality was observed during the 7-day chronic test, but survival gradually decreased with increasing Hg concentrations. No individuals survived at the end of the test at Hg concentrations ≥17,500 ng L^{-1}. The IC25 was determined as 2,109 ng Hg L^{-1} for survival.

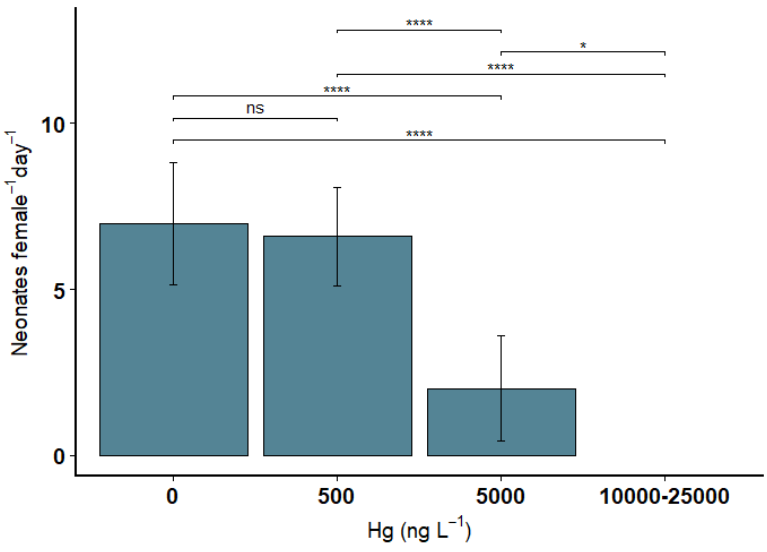

Figure 24. Reproduction rate (expressed as neonates survival female^{-1} d^{-1}) of Ceriodaphnia dubia exposed to a gradient of dissolved Hg concentrations.

Reproduction rate also strongly depended on the Hg concentrations with a clear decrease in the number of neonates produced by a surviving female per day with values of 4.0–9.4 neonates $female^{-1}$ d^{-1} when daphnia were exposed to Hg concentrations ≤500 ng L^{-1}. Average reproduction rate was reduced by 70% (0.0–4.4 neonates $female^{-1}$ d^{-1}) at 5,000 ng Hg L^{-1} compared with the control condition (Figure 24). No reproduction was observed at Hg concentrations ≥17,500 ng L^{-1}. IC25 was determined as 888 ng Hg L^{-1} for reproduction.

During this experiment, growth of daphnia from the different treatments was regularly followed. Because of the low survival at the highest Hg concentrations, growth was measured throughout the test for the treatments at 0, 500, and 5,000 ng Hg L^{-1}. Growth kinetics were best fitted using linear models (R^2: 0.94–0.96), and a significant

difference in slopes was found when daphnia were exposed to 5,000 ng L^{-1} with a significant reduction of the length at the end of the experiment (0.94 ± 0.05 mm against 1.12 ± 0.04 mm for the control and 500 ng Hg L^{-1} treatments) (Figure 25).

Altogether, these results are useful to provide a BL of the effects of aqueous Hg on a model aquatic invertebrate species, allowing further investigations regarding the efficiency of Hg mitigation strategies.

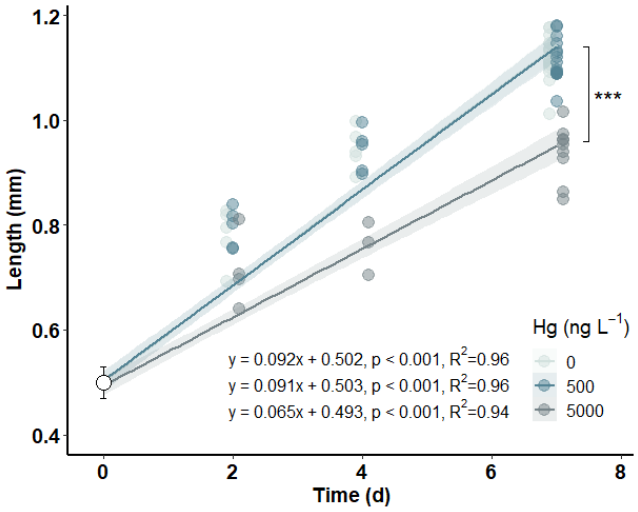

Figure 25. Length (from the top of the eye to the base of the spine) of Ceriodaphnia dubia exposed to a gradient of dissolved Hg concentrations.

Mercury Biokinetics in EFPC Fish

As stated previously, the primary goal of the ecological manipulation task is to reduce Hg bioaccumulation in fish in EFPC. This year, we started examining a biokinetic model to estimate Hg in fish incorporating many dynamic natural factors. The biokinetic model, known in the literature as the "DYMBAM model" (e.g., Luoma and Rainbow 2005), predicts the concentration of a contaminant (here, Hg) within an organism (C_t) based on two modes of influx and two of efflux. The internal concentration of Hg (C_t) increases from aqueous exposure (I_W) and through ingestion of contaminated food (I_F). The internal Hg concentration decreases from the rate of efflux (the organism excreting Hg in some way at a rate k_e) and from growth (at a rate g). The latter is referred to as "dilution due to growth"—as the organism grows, the contaminant is diluted because of an increase in biomass (the denominator of the internal concentration, C_t). The equation is defined below with parameters listed in Table 2.

$$\frac{dC_t}{dt} = (I_W + I_F) - (k_e + g)C_t \text{ with } I_W = k_u C_w \text{ and } I_F = AE * IR * C_F$$

Table 2. Parameters of the Biokinetic model.

	Parameter	Units	Source of value
k_u	Uptake rate of Hg into from water	L/(g_{fish} × d)	Literature
k_e	Efflux rate of Hg from fish into water	1/d	Literature
g	Growth rate	1/d	Estimated from our mark recapture data
C_W	Hg concentration in water	mg_{Hg}/L	EFPC data
C_F	Hg concentration in food	mg_{Hg}/g_{food}	EFPC data
AE	Assimilation efficiency	—	Literature
IR	Ingestion rate	$g_{food}/(g_{fish}$ × d)	Literature

The data for this model include Hg concentrations from EFPC fish (redbreast sunfish and rock bass) collected by our group from 2008 to 2018. These EFPC data include many fish that have been PIT-tagged and recaptured so that we can compare Hg levels in recaptured and one-time measurement data. They also incorporate data from an extensive literature search to identify parameter values for the model (Table 3).

Table 3. Brief summary of a literature review of Hg biokinetic studies in multiple species of fish.

Form of Hg	Dietary parameter	Freshwater	Marine
Hg	AE (%)	8.5–51.3	10.4–38
	k_e (d^{-1})	0.003–0.042	0.026–0.104
	k_u (ml g^{-1} d^{-1})	38–78	5–305
^{203}Hg	AE (%)	13.2–35	1.9–43
	k_e (d^{-1})	0.039–10.5	0.071–0.131
	k_u (ml g^{-1} d^{-1})	86	15–80
	Half-life (days)	18	—
MeHg	AE (%)	32–98	55.6–95.4
	k_e (d^{-1})	0.0042–0.021	0.0018–0.024
	k_u (ml g^{-1} d^{-1})	185–1,280	350–1,900
^{203}MeHg	AE (%)	50–95.4	10–99
	k_e (d^{-1})	0.0055	0.004–0.02
	k_u (ml g^{-1} d^{-1})	333	1,155–4,375

Successful parametrization of this biokinetic model to our data on EFPC would enable us to predict the concentration of Hg in fish based on the aqueous and dietary concentrations of Hg in EFPC. Analysis of this model will also allow us to quantitatively compare the relative effect of aqueous and dietary exposure of Hg on the Hg concentration in fish. Additionally, we are working on parametrizing this model separately for MeHg and total Hg, facilitating the direct comparison of the two forms of Hg on bioaccumulation in fish. Furthermore, we could use this model in the future to estimate the aqueous and dietary concentrations of Hg in EFPC needed to achieve the desired reduction of Hg contamination in biota necessary to meet the NRWQC. Identifying these target concentrations is crucial to estimate the number of bivalves needed in EFPC to decrease aqueous Hg concentrations to a level that will meaningfully affect concentrations of Hg in EFPC fish.

Future Needs: Ecological Manipulation

Within this task, several areas of continuing and new research are warranted. Because periphyton serve as the base of the food chain and are likely a significant factor contributing to MeHg production and bioaccumulation in EFPC, understanding periphyton dynamics (e.g., standing stock biomass, growth rate) is critical. We have collected data on Hg inventories in periphyton and are working on methods (potentially using remote sensing) to characterize biomass in the stream. In the laboratory, we will begin preliminary growth of periphyton from EFPC water soon, which will allow us to investigate natural species from the creek under controlled conditions.

The bivalve species living in the lab currently in numbers available for experiments include Asian clam and young Pocketbook (*L. ovata*). We plan to repeat filtration experiments on more species when we can coordinate with TWRA to acquire them. This was planned for summer 2020, but pandemic travel restrictions postponed it.

Further laboratory, field, and modeling work is needed to better understand the factors affecting mussel and clam filtration and Hg removal rates, and to determine the implications of mussel filtration on Hg methylation. Although experiments to date have focused on filtration rates, upcoming experiments will focus on Hg removal and bioaccumulation rates. Critical to this discussion is a modeling exercise to determine the density of mussels needed to effect Hg removal in the stream and whether the food web in EFPC could support such a density. These studies will rely heavily on the use of the renovated stream mesocosms that were a part of the AEL upgrade. Finally, additional modeling work is needed to evaluate the potential of additions or removals of fish or mussel species to mitigate Hg trophic transfer in the stream.

Watershed Modeling

Background

A more quantitative, integrated understanding of current and future sources and dynamics of Hg in EFPC is necessary to facilitate science-informed strategies for Hg remediation and research needs. The purpose of the watershed modeling task for EFPC is to collect, collate, and integrate relevant information from past and ongoing laboratory and field Hg remediation research campaigns, integrate the Hg data with a geospatial characterization database for the EFPC watershed (Figure 26), and then use these integrated data sets as foundational inputs to a multi-platform watershed model. Like any watershed contaminated with Hg, transport and transformation of Hg in EFPC is controlled by processes and pathways that connect the upland, floodplain, and in-stream environments. These processes provide the conditions for the production of MeHg and bioaccumulation of Hg and MeHg in different trophic levels of the food chain in the upland-to-stream continuum. Therefore, the integration of different models that can represent these processes and pathways and provide insight into the continuum is essential. We use a sequential combination of three different models: a model that captures the landscape hydrology of EFPC and simulates transportation of Hg across the landscape to the stream, a hydraulic stream model that describes in-stream movement and processing of Hg, and a model that describes bioaccumulation of Hg across different trophic levels in the aquatic ecosystem of EFPC. Where appropriate, UEFPC is modeled separately from LEFPC because of the very different land use and hydrologic characteristics of the upper and lower portions of the watershed. The watershed-scale modeling enables incorporation of information from the various components of the land-stream continuum—including the upland, floodplain, land-water interface, and stream environments—at high spatial and temporal resolution and improves process-level identification of hot spots and moments of Hg source and movement and transformation of Hg within the watershed. The watershed-scale modeling of Hg dynamics facilitates the ex-ante evaluation of the efficacy of technologies to prioritize remedial options to reduce Hg contamination in the environment.

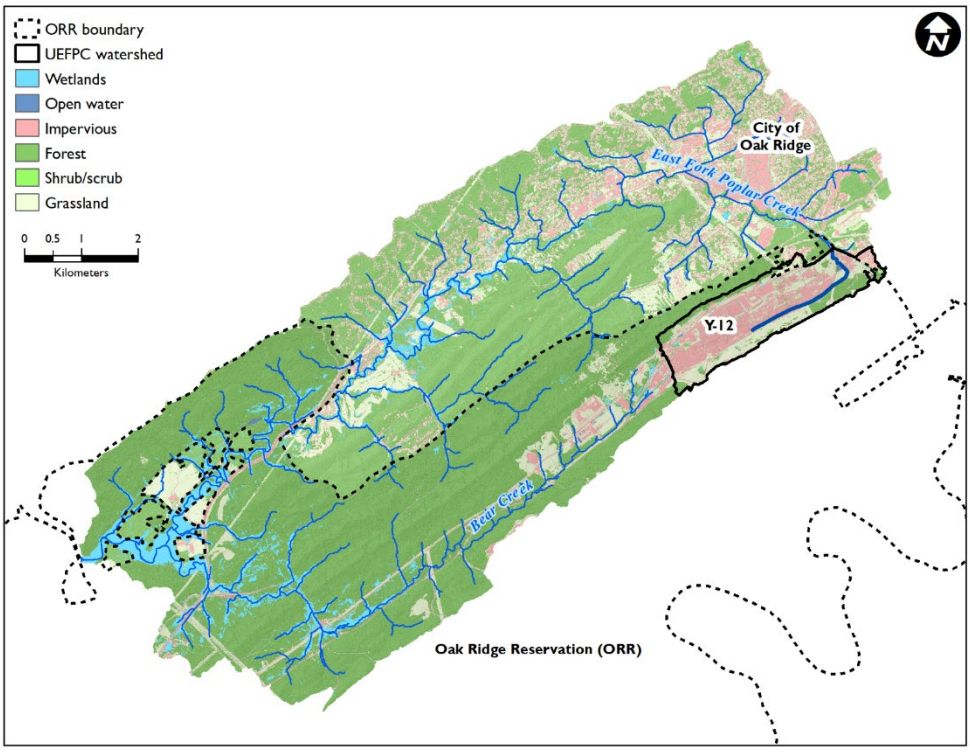

Figure 26. EFPC watershed.

Watershed Modeling Approach

A statistical analysis of UEFPC and LEFPC hydrology showed that two flow regimes exist in UEPFC: a controlled surface flow during a low or no rainfall period and a stochastic stream flow during high and intense precipitation events.

These two hydrological regimes are both influenced by industrial land use in the watershed along with the intensive flow management practices adopted to reduce Hg loading from the watershed. Once MTF is operational, flow and Hg loading in UEFPC will be severely constrained, except for intense rain events where flow at OF200 is higher than inflow capacity or the treatment and storage capacity of MTF. In LEFPC, diverse land use exists that is dominated by urban and forested land cover with little or no flow mediation other than added flow from the wastewater treatment plant. Additionally, streambanks and floodplains are the major Hg-contributing areas in LEFPC and thus, LEFPC Hg dynamics are heavily influenced by stochastic flow events. A single Soil and Water Assessment Tool (SWAT) model for the EFPC watershed would hinder the ability of the model to simulate the various management needs for UEFPC and LEFPC. Consequently, different SWAT models were developed for UEFPC and LEFPC and were sequentially linked together by inputting outflow from UEFPC as a point source to the LEFPC model.

SWAT is a physically based, watershed-scale, continuous-time simulation model that integrates climate, soil, and topography on daily and sub-daily time steps and allows for simulation of different flow and sediment management practices (Arnold et al. 1998). SWAT divides watersheds into smaller sub-basins that are further categorized into one or more unique hydrologic response units (HRUs) with similar soil type, land use, slope, and land management practices. The number of HRUs in a watershed is decided by user-defined criteria. SWAT calculates the water balance components (e.g., evapotranspiration, surface, sub-surface flow) for each HRU and aggregates to the sub-basin while also accounting for human modification like water extraction, augmentation, storage, and diversion. The key inputs for the SWAT model (Table 4) are to characterize topography and delineate the watershed and sub-watersheds; climate data including temperature and precipitation; and land cover. Additionally, point-source water/pollution inputs to the watershed can be included to represent human influence on hydrology and water quality.

Table 4. Example data inputs and sources for initial SWAT setup.

Data input	Spatial resolution	Source
Digital elevation model	0.76 m	Created using lidar data
Climate	Stations in the UEPFC	Oak Ridge Reservation Weather[a]
STATSGO	Medium	US Department of Agriculture[b]
Land cover	30 m	US Geological Survey[c]
National Hydrography Dataset	1:250k	NHDPlus Version 2[d]

[a] https://metweb.ornl.gov/page5.htm
[b]https://datagateway.nrcs.usda.gov/
[c]https://www.mrlc.gov/data
[d] https://www.epa.gov/waterdata/nhdplus-national-hydrography-dataset-plus

For UEFPC, the goal of the watershed modeling was to develop a mercury load assessment tool (M-LAT). An empirical process–based modeling approach was followed similar to the US Geological Survey Spatially Referenced Regressions on Watershed attributes (SPARROW) model for water quality. SWAT was used to characterize hydrology and sediment transport characteristics, which were subsequently used in a regression analysis to relate simulated flow and sediment with Hg in water and sediment from field-scale measurements in the watershed. For LEFPC, a SWAT model was developed to generate sub-watershed hydrology and sediment loading, which were then used as inputs for US Army Corps of Engineers Hydrologic Engineering Center River Analysis System (HEC-RAS) 2D stream modeling.

UEFPC Modeling

Empirical Modeling of Hg Loading

Flow and sediment data for calibration and validation of the UEFPC SWAT model were obtained from long-term monitoring data stored in the Oak Ridge Environmental Information System database. A sequential estimation of an Hg loading function for monitoring points (i.e., outfalls and Station 17) was performed for UEFPC. UEFPC is often divided into west-end and east-end sub-watersheds, with OF200 and Station 17 representing the outlet points of the west-end and east-end sub-watersheds, respectively. Mercury flux (g day^{-1}) from each of the outfalls contributing to OF200 (i.e., OF169, OF163, OF160, and OF150) was empirically linked to flow from these outfalls.

The function used to estimate Hg flux at OF200 is

$$\widehat{\mathrm{Hg}}_{\mathrm{OF200}} = f\left(\mathrm{Flow}_{\mathrm{OF200}}, \widehat{\mathrm{Hg}}_{\mathrm{OF169}}, \widehat{\mathrm{Hg}}_{\mathrm{OF163}}, \widehat{\mathrm{Hg}}_{\mathrm{OF160}}, \widehat{\mathrm{Hg}}_{\mathrm{OF150}}\right) \quad (1)$$

The function used to estimate Hg flux at Station 17 is

$$\widehat{\mathrm{Hg}}_{\mathrm{St17}} = f\left(\mathrm{Flow}_{\mathrm{St17}}, \mathrm{Sediment}_{\mathrm{St17}}, \widehat{\mathrm{Hg}}_{\mathrm{OF200}}, \mathrm{SCV}, \mathrm{WA}\right) \quad (2)$$

where $\widehat{\mathrm{Hg}}$, Flow, and Sediment represent Hg flux or concentration, flow, and sediment load at monitoring points, respectively, SCV represents control variables for isolating the influence of season, WA is a binary dummy variable that represents active/inactive flow augmentation to the creek, and HI represents human intervention effects on flow and sediment load. Human intervention is introduced to capture occasional higher flow/sediment load events at monitoring points that do not coincide with higher rainfall or WA. For each of the monitoring points, regressions with linear, quadratic, semi-log, and log-log forms were estimated with Hg flux as the dependent variable using stepwise regression with a p-value of 0.05 as the parameter selection criteria. The model with the highest R^2 value was selected to represent Hg loading from each monitoring point. After the Hg empirical functions were established, the model was used to simulate different scenarios.

Scenarios

Scenarios are narrative statements of possible future events that influence the drivers of a system. In modeling, scenario-based analysis is used to create specific "what-if" situations in a given the context. The scenario might simultaneously constrain or relax one or more driving variables to elucidate the effect of variables of interest on a system if a specific event occurred in the future. In this study, three drivers—precipitation, land use change, and a technical remediation solution (MTF)—were used to develop a nine scenario narrative using three precipitation intensities (current, extreme wet and extreme dry), two land use contexts (current and the proposed 2040 land use change for Y-12 and UEFPC) and an operational surface water collection and treatment system (Table 5). The extreme wet (163 mm rainfall) and extreme drought (26 consecutive dry days with <1 mm precipitation) precipitation scenarios were estimated using the Generalized Extreme Value Distribution (GEV) with a return period of 100 years of historical rainfall data from 1970 to 2019. The proposed 2040 future land use has significantly less impervious surface than the current watershed and should thus reduce stormwater runoff to the creek during rainfall events. MTF is under construction in UEFPC and once completed will have the capacity to collect a maximum inflow (stormflow + base flow) of up to 40,000 gpm, a storage capacity of 2 million gallons, and the ability treat up to 3,000 gpm.

Table 5. List of scenarios for UEFPC modeling.

	Scenario	Active MTF	Precipitation			Land cover	
			Normal	Extreme	Drought	Current	2040
1	BL: current land cover, normal precipitation		x			x	
2	BL: current land cover, extreme precipitation			x		x	
3	BL: current land cover, drought				x	x	
4	Active MTF, current land cover, normal precipitation	x	x			x	
5	Active MTF, current land cover, extreme precipitation	x		x		x	
6	Active MTF, current land cover, drought	x			x	x	
7	Active MTF, 2040 land cover, normal precipitation	x	x				x
8	Active MTF, 2040 land cover, extreme precipitation	x		x			x
9	Active MTF, 2040 land cover, drought	x			x		x

Results

Flow and sediment calibration, validation and evaluation

To calibrate the UEFPC SWAT model, different parameters were adjusted that control watershed hydrology and sediment loading, including evapotranspiration, runoff generation processes, soil water holding capacity, and sub-surface drainage. The calibration and validation showed a good model fit of daily, monthly, and annual surface flow values and sediment load (Figure 27A–D).

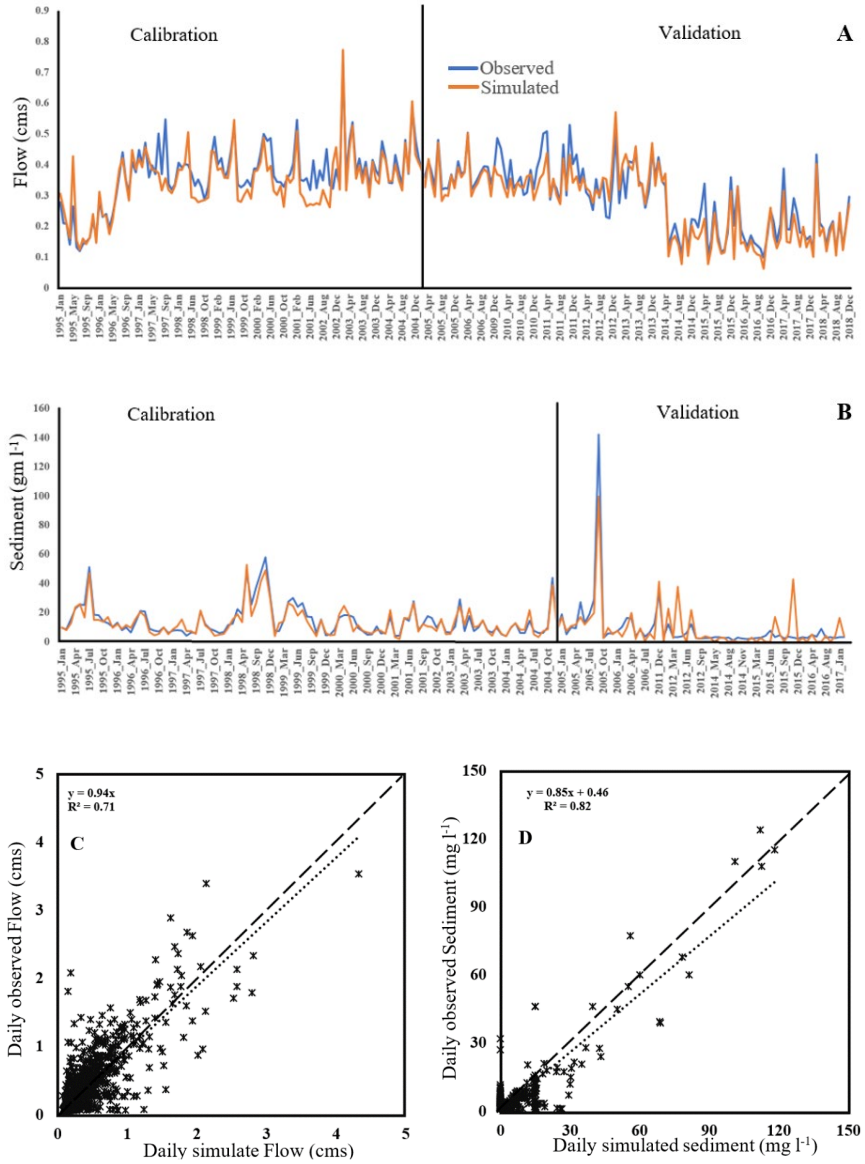

Figure 27. Calibration and validation of (A) monthly flow, (B) monthly sediment, and (C) daily flow at Station 17; (D) calibration and validation of daily sediment load at C11.

Mercury Loading Function for OF200 and Station 17

The regression analysis of Hg flux from OF200 showed that flow is the major driver of Hg flux in the west-end of the UEFPC watershed, whereas both flow and sediment significantly contributed to Hg flux at Station 17. Data for both OF200 and Station 17 showed that a log-log relationship exists between Hg flux and flow, and for sediment for Station 17. Furthermore, both Hg flux regressions showed a high predictive ability with an adjusted R^2 value of 0.71 and 0.78, respectively, for OF200 and Station 17 (Tables 6 and 7). A two-fold cross-validation was applied for these

regression models, which revealed that the models are robust against sample size and composition (Figure 28). Furthermore, the estimated Hg flux function for OF200 showed a significant influence of OF163, OF169, and OF150 on Hg flux from OF200. The Hg flux from Station 17 is heavily influenced by flow and sediment at Station 17, Hg flux from OF200, WA, the interaction between WA with sediment at Station 17, and Hg flux from OF200.

Table 6. Estimated Hg function for OF200.

	Regression coefficient	't value
Intercept	−0.91	−4.78
OF163	0.26	6.51
OF150	0.23	4.60
OF169	0.18	2.21
OF160	0.12	0.92
Log-Log and Adj R^2 = 0.71		

Table 7. Estimated Hg Function for Station 17.

	Regression coefficient	't value
Intercept	2.72	1.32
Flow at Station 17	0.51	2.22
Sediment at Station 17	0.34	3.87
OF200 Hg	0.65	2.75
OF200 Flow	0.77	3.11
WA	1.381	3.17
WA X Flow Station 17	−0.47	−1.92
WA X Sed Station 17	0.31	1.52
Log-Log and Adj R^2 = 0.78		

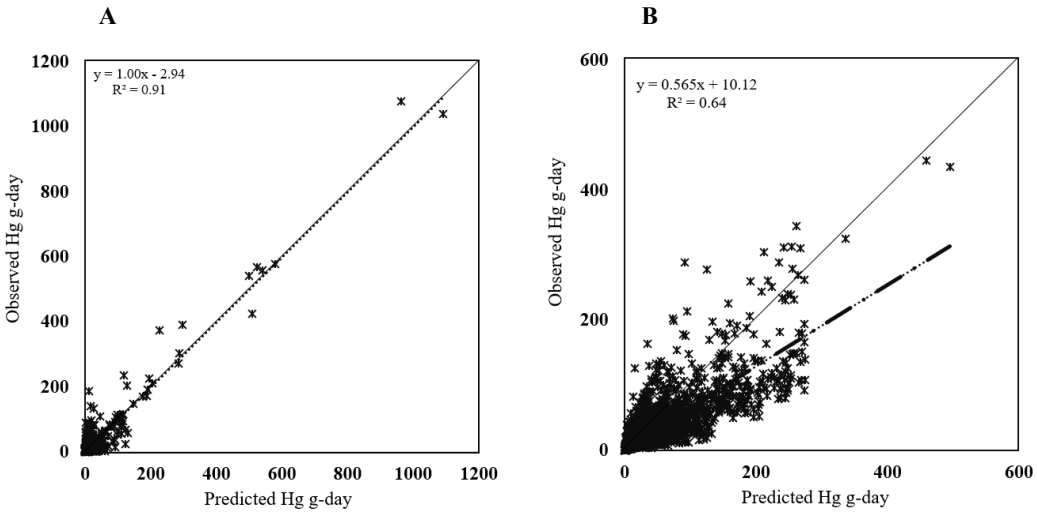

Figure 28. (A) Predicted and observed Hg load from (A) Station 17 and (B) OF200.

Scenario Analysis

Normal precipitation scenarios

A 10-year data record from 2009 to 2018 served as the rainfall input for the three scenarios with normal precipitation: (1) current land cover with no MTF, (2) current land cover with MTF operational, and (3) 2040 land cover with an

operational MTF. During this period, there was very high precipitation in September 2011 and November 2016 and a four-week long drought in October and November 2016. The results showed that average daily Hg flux over this period is 28.82 g-day. The monthly distribution of Hg flux (Figure 29) shows that the second half of the year contributes higher than early months of the year, in general.

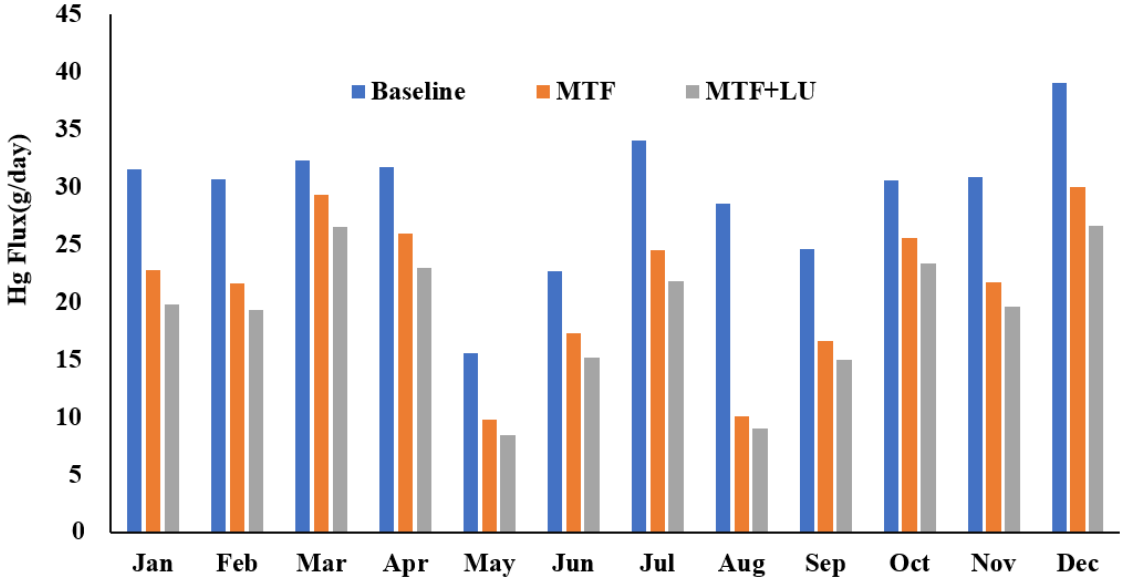

Figure 29. Average daily Hg load for month under normal precipitation for BL, BL with MTF (MTF), and BL, MTF, and land use (LU) 2040 scenarios.

Simulation of drought, 26 days of continuous dry days, and extreme precipitation of 163 mm rainfall showed that drought would result in ~50% reduction in daily Hg loading compared with the normal precipitation while extreme precipitation increase daily Hg flux by 3 times that of normal precipitation (Figure 30).

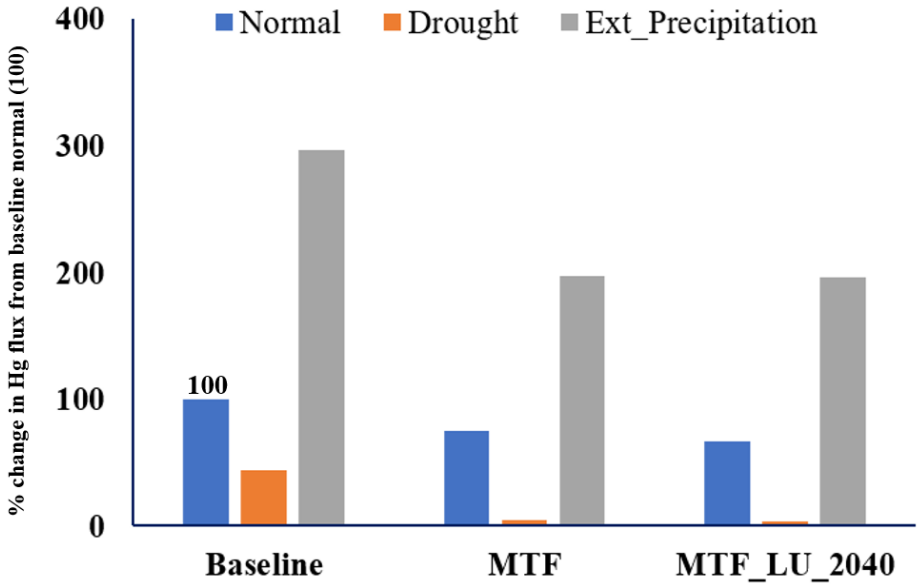

Figure 30. A comparison of average daily Hg load of normal, extreme dry and extreme precipitation scenario for BL, MTF, and BL, MTF, and land use (LU) 2040.

BL + MTF Scenario

Once MTF starts operating, the total daily volume of water that can be treated (3,000 g/m × 60 × 24 = 4.32 MG) and stored by MTF (200,000 g) is 6.32 MG. Thus, if OF200 receives >6.32 MG in a day, the rest of the flow will be diverted

away from MTF. The flow simulation at OF200 showed that 84.83% of the simulation days, average daily flow is <3,000 g/m. Additionally, 90.52% of the days flow at OF200 are less than 6.32 MG. However, none of the cases at OF200 generated a flow >40,000 g/m.

A simulation analysis was conducted to understand rainfall and flow generation at OF200. The result showed that 13.57 mm of rainfall is enough to generate the 3,000 g/m flow (Figure 31). The generated flow also includes water used by the plant for other purposes. Furthermore, MTF would treat these volumes of flow with Hg concentration 15.42 Hg g-day to reduce it to 1.42 (200 ng effluent Hg concentration of MTF) with an average annual flow of 707.28 MG. Additionally, simulation results showed that 9.36% of days' flow at OF200 is more than their daily capacity (6.32 MG), and 3.14% days' flow at OF200 will have >6.32 MG flow consecutive days. Additionally, average yearly non-captured water for the days with >6.32 MG is 252.77 MG with an average 56.81 g-day Hg concentration. During drought conditions, all the available flow will be used by MFT. Thus, comparing with and without MTF, MTF would be able to treat all the Hg flux from OF200 during drought. However, SWAT simulations showed that extreme rainfall would create 44,650.3 g/min flow was generated at OF200, which is above the designed capacity of inflow to MTF. While comparing with and without MTF under normal precipitation, by assuming full efficiency of the system, MTF would be able to reduce daily Hg flux to 21.7 g-day with MTF.

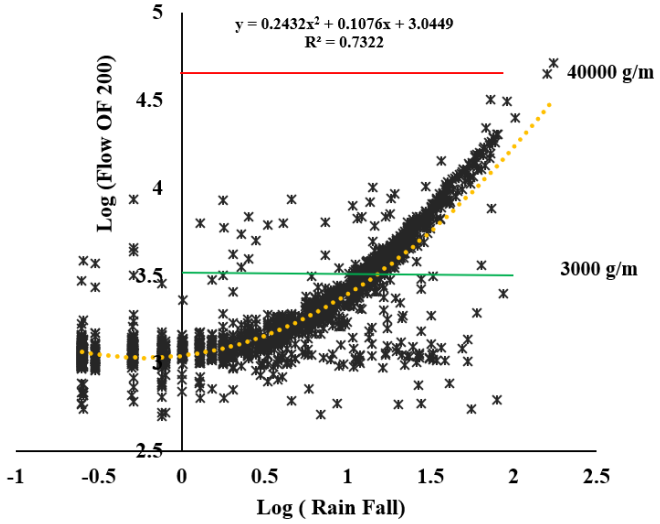

Figure 31. Relationship between rainfall and simulated flow at OF200.

BL + MTF + 2040 Land Use

Implementing more green coverage and less impervious land would reduce the surface flow generation. Simulation of 2040 land use in SWAT with normal precipitation showed an increased number of days with <6.32 MG/day flow at OF200 along with an increased number of days with <3,000 g/m flow at OF200. As a greater number of days with flow feeding into MTF, Hg concentration of 1.42 Hg g-day would be reduced to 1.13 Hg g-day. Additionally, flow will reduce by 10.26% at Station 17. However, extreme precipitation can still produce >40,000 g/m flow at OF200. The changes in flow brought by 2040 land use would result in a reduction in daily Hg flux to 19.24 g-day.

One of the major obstacles in heavy metal remediation activities is the lack of availability of models at a suitable scale. Therefore, model-informed decision-making in Hg remediation is needed. Additionally, a general Hg cycling model might not be suitable for unique watersheds like UEFPC, where human mediation of Hg movement is widespread, along with the elevated concentration of other reactive and nonreactive elements, including nitrogen, phosphorus, and zinc. This study demonstrated the usefulness of an integrated watershed simulation model with a statistical Hg loading function modeling in understanding long-term Hg load reduction associated with the potential remediation strategies. Therefore, the model can be used to answer what-if questions related to the management of Hg loading from UEFPC and trade-off analysis for different remediation decisions. The SWAT-UEFPC model is currently running on a daily time step. However, for sub-daily events such as extreme precipitation, a SWAT-UEFPC model for sub-daily time step would be ideal.

SWAT model for LEFPC

SWAT modeling for the LEFPC is progressing now, where simulated flow and sediment load from SWAT-UEFPC will be added as a point source. The relevant data include digital elevation mode, land-use, soil, and weather derived from the same data source used for developing the SWAT-UEFPC (Figure 32). The focus of the SWAT-LEFPC work will be to understand how variable flow and land use change across the LEFPC influence Hg load to the stream. Model building is progressing and expected to be complete in September 2021. The SWAT-LEFPC will be calibrated and validated by mid-November and simulation of scenarios will be implemented by end of 2021.

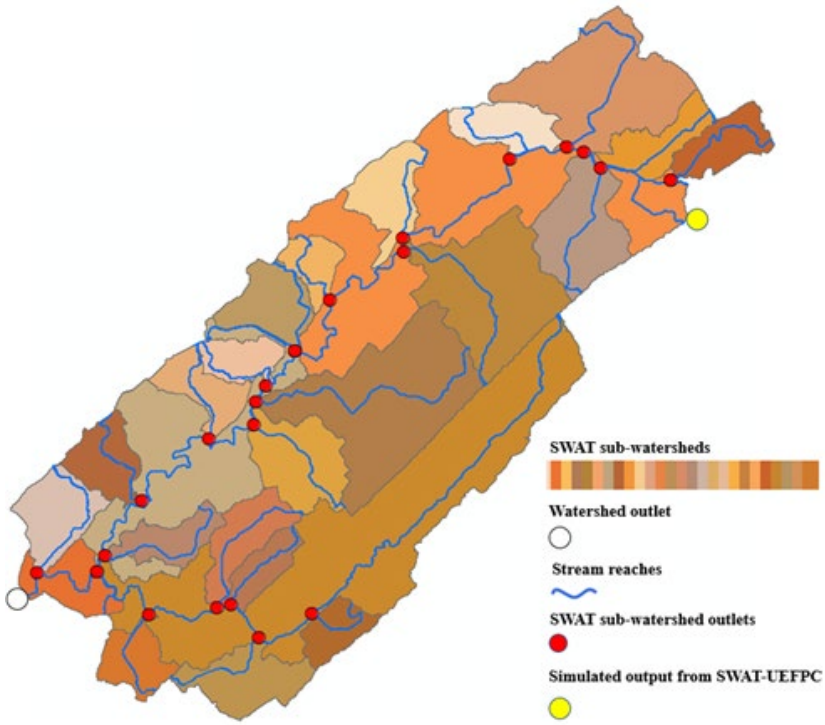

Figure 32. LEFPC watershed developed in SWAT.

Conclusions and Future Directions

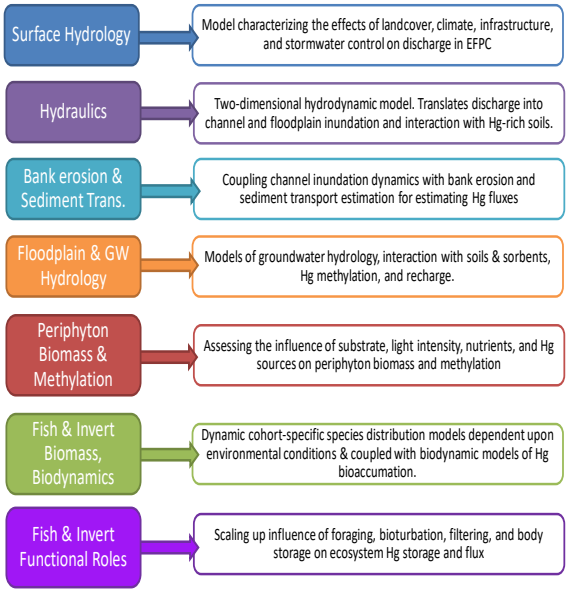

Figure 33. EFPC Ecosystem Model Compartments informing the understanding of the EFPC watershed ecosystem using SWAT and HEC-RAS.

Significant scientific and technological progress has been made during the 5 years of the Mercury Remediation Technology Development project. A strategy was developed early in the program that is consistent with the adaptive management paradigm and DOE's technology readiness level guidelines. Initially, field studies were prioritized to better understand the Hg sources, transformations, transport, and fate processes in the EFPC system. Systems-level studies have pointed to the importance of stream bank soils—and especially HRDs—in the upstream section of EFPC as a source of Hg to the creek, the relatively small role of groundwater and floodplain sources, the importance of flow and other water chemistry and particle characteristics on the form of Hg, the importance of periphyton on Hg methylation, and the role of MeHg found in prey species on fish receptors. A watershed approach to EFPC remediation is being used because it considers all the contributing factors that affect Hg transformations in the environment. Quantitative modeling received a significant focus in FY 2020 to simulate remediation and technology development scenarios and better inform future remedial decision-making (Figure 33). Understanding the potential outcomes of environmental change could lead to opportunities for decreasing Hg risks while also managing and restoring the stream for natural resource benefits and/or water quality improvement.

With a better spatial and temporal understanding of the watershed system, specific technologies and strategies are being assessed as potential abatement actions. Studies have been conducted to evaluate alternative treatment chemicals on Hg flux, the role of sorbents on Hg and MeHg with DOM, and the use of bivalves as a tool for reducing particle-associated Hg in the water column.

Figure 7. AEL at ORNL.

Future directions for Hg research and technology development in LEFPC will include (1) targeted field studies to inform key process and research questions, (2) enhancement of our watershed-scale understanding through quantitative modeling, (3) a greater emphasis on mesoscale studies of potential technologies in the upgraded AEL (Figure 34), and (4) remediation and technology simulation to inform the LEFPC remedial alternatives evaluation in the mid-2020s. In FY 2020, the design and construction of new experimental capabilities in the AEL at ORNL was completed. The modernized facility will provide a unique capability to evaluate Hg remediation technologies in a variety of source waters. Laboratory studies in the AEL will commence in FY 2021 and will advance the scale of testing beyond field studies and bench-scale testing.

Abbreviations

ADCP	acoustic Doppler current profiler
AEL	Aquatic Ecology Laboratory
BL	baseline
DOC	dissolved organic carbon
DOE	US Department of Energy
DOM	dissolved organic matter
EFK	East Fork Poplar Creek kilometer
EFPC	East Fork Poplar Creek
HEC-RAS	US Army Corps of Engineers Hydrologic Engineering Center River Analysis System
Hg	mercury
Hgi	inorganic mercury
HgT	total mercury
HRD	historical release deposit
LEFPC	lower East Fork Poplar Creek
Mn	manganese
MeHg	methylmercury
MTF	Mercury Treatment Facility
NOAA	National Oceanic and Atmospheric Administration
NRWQC	National Recommended Water Quality Criterion
OF	Outfall (use only with numbered items/outfalls, as in OF200)
ORNL	Oak Ridge National Laboratory
SWAT	Soil and Water Assessment Tool
TRL	technology readiness level
TWRA	Tennessee Wildlife Resource Agency
UEFPC	upper East Fork Poplar Creek
Y-12	Y-12 National Security Complex

References

Acha, D., Pabon, C. A., and Hintelmann, H. 2012. "Mercury methylation and hydrogen sulfide production among unexpected strains isolated from periphyton of two macrophytes of the Amazon." *FEMS Microbiology Ecology* 80(3): 637–645. doi: 10.1111/j.1574-6941.2012.01333.x.

Agatz, A., Hammers-Wirtz, M., Gergs, A., Mayer, T. and Preuss, T.G., 2015. "Family-portraits for daphnids: scanning living individuals and populations to measure body length." *Ecotoxicology* 24: 1385–1394.

Arnold, J. G., Srinivasan, R., Muttiah, R. S., and Williams, J. R. 1998. "Large Area Hydrologic Modeling and Assessment Part I: Model Development." *Journal of the American Water Resources Association* 34(1): 73–89.

Bates, D., Machler, M., Bolker, B., and Walker, S. 2015. "Fitting linear mixed-effects models using lme4." *Journal of Statistical Software* 67(1): 1–48. doi: 10.18637/jss.v067.i01.

Brooks, S., Virginia, E., Dickson, J., Earles, J., Lowe, K., Mehlhorn, T., Olsen, T., DeRolph, C., Watson, D., and Peterson, M. 2017. *Mercury Content of Sediments in East Fork Poplar Creek: Current Assessment and Past Trends*. ORNL/TM-2016/578. Oak Ridge National Laboratory, Oak Ridge, Tennessee. doi: 10.2172/1338545.

Brooks, S. C., Lowe, K. A., Mehlhorn, T. L., Olsen, T. A., Yin, X., Fortner, A. M., and Peterson, M. J. 2018. *Intraday water quality patterns in East Fork Poplar Creek with an emphasis on mercury and monomethylmercury*. ORNL/TM-2018/812. Oak Ridge National Laboratory, Oak Ridge, Tennessee. doi: 10.2172/1437608.

Chasar, L. C., Scudder, B. C., Stewart, A. R., Bell, A. H., and Aiken, G. A. 2009. "Mercury cycling in stream ecosystems. 3. Trophic dynamics and methylmercury bioaccumulation." *Environmental Science & Technology* 43: 2733–2739.

Chen, X. B., Feng, X. D., Liu, J., Fryxell, G. E., and Gong, M. L. 1999. "Mercury separation and immobilization using self-assembled monolayers on mesoporous supports (SAMMS)." *Separation Science and Technology* 34(6–7): 1121–1132.

DeRolph, C., et al. 2019. *Conceptual Model Update of Mercury Sources and Flux at Y-12 and Upper East Fork Poplar Creek, Oak Ridge, Tennessee.* ORNL/TM-2019/1356. Oak Ridge National Laboratory, Oak Ridge, Tennessee.

Dickson, J. O., Mayes, M. A., Brooks, S. C., Mehlhorn, T. L., Lowe, K. A., Earles, J. K., Goñez-Rodriguez, L., Watson, D. B., and Peterson, M. J. 2019. "Source relationships between streambank soils and streambed sediments in a mercury-contaminated stream." *Journal of Soils and Sediments* 19(4), 2007–2019.

Dittman, J. A., Shanley, J. B., Driscoll, C. T., Aiken, G. R., Chalmers, A. T. and Towse, J. E. 2009. "Ultraviolet absorbance as a proxy for total dissolved mercury in streams." *Environmental Pollution* 157: 1953–1956.

DOE (US Department of Energy). 2017a. *Strategic Plan for Mercury Remediation at the Y-12 National Security Complex, Oak Ridge, Tennessee.* DOE/OR/01-2605&DR/R1. Oak Ridge Office of Environmental Management.

DOE (US Department of Energy). 2017b. *Mercury Technology Development Plan for Remediation of the Y-12 National Security Complex and East Fork Poplar Creek, Oak Ridge, Tennessee.* DOE/ORO-2489/Rev. 1. Oak Ridge Office of Environmental Management.

Farrell, R. E., Huang, P. M., and Germida, J. J. 1998. "Biomethylation of mercury(II) adsorbed on mineral colloids common in freshwater sediments." *Applied Organometallic Chemistry* 12: 613–620.

Fox, J. and Weisberg, S. 2019. *An R Companion to Applied Regression*, Third edition. Sage, Thousand Oaks, California. https://socialsciences.mcmaster.ca/jfox/Books/Companion/

Goodwin, N. R., Armston, J. D., Muir, J., and Stiller, I. 2017. "Monitoring gully change: A comparison of airborne and terrestrial laser scanning using a case study from Aratula, Queensland." *Geomorphology* 282: 195–208.

Graham, A. M., Aiken, G. R., and Gilmour, C. C. 2013. "Effect of Dissolved Organic Matter Source and Character on Microbial Hg Methylation in Hg–S–DOM Solutions." *Environmental Science & Technology* 47: 5746–5754.

Hansen, B. W., Dolmer, P., and Vismann, B. 2011. “In situ method for measurements of community clearance rate on shallow water bivalve populations.” *Limnology and Oceanography-Methods* 9: 454–459. https://doi.org/10.4319/lom.2011.9.454

Hills, A., Pouil, S., Hua, D., and Mathews, T. 2020. “Clearance rates of freshwater bivalves *Corbicula fluminea* and *Utterbackia imbecilis* in the presence and absence of light.” *Aquatic Ecology* 54: 1059–1066. https://doi.org/10.1007/s10452-020-09793-7

Hines, M. E., Horvat, M., Faganeli, J., Bonzongo, J.-C. J., Barkay, T., Major, E. B., Scott, K. J., Bailey, E. A., Warwick, J. J., and Lyons, W. B. 2000. “Mercury biogeochemistry in the Idrija River, Slovenia, from above the mine into the Gulf of Trieste.” *Environmental Research Section A* 83: 129–139.

Homer, C. G., et al. 2015. “Completion of the 2011 National Land Cover Database for the conterminous United States-Representing a decade of land cover change Information.” *Photogrammetric Engineering and Remote Sensing* 81(5): 345–354.

Horvat, M., et al. 2003. “Total mercury, methylmercury and selenium in mercury polluted areas in the province Guizhou, China.” *Science of the Total Environment* 304: 231–256.

Hydrologic Engineering Center. 2016. *HEC-RAS, River Analysis System, Version 5.03*. US Army Corps of Engineers, Davis, California.

Jackson, T. A. 1989. “The influence of clay minerals, oxides, and humic matter on the methylation and demethylation of mercury by micro-organisms in freshwater sediments.” *Applied Organometallic Chemistry* 3(1): 1–30.

Johs, A., Eller, V. A., Mehlhorn, T. L., Brooks, S. C., Harper, D. P., Mayes, M. A., Pierce, E. M., and Peterson, M. J. 2019. “Dissolved organic matter reduces the effectiveness of sorbents for mercury removal.” *Science of the Total Environment*, 690: 410–416.

Joslin, J. D. 1994. “Regional differences in mercury levels in aquatic ecosystems- A discussion of possible causal factors with implications for the Tennessee River System and the Northern Hemisphere.” *Environmental Management* 18: 559–567.

Kelly, C. A., Rudd, J. W. M., Louis, V. L., and Heyes, A. 1995. “Is total mercury concentration a good predictor of methylmercury concentrations in aquatic systems.” *Water Air and Soil Pollution* 80(1–4): 715–724.

Kiesel, J., Schmalz, B., Brown, G., and Fohrer, N. 2013. “Application of a hydrological-hydraulic modelling cascade in lowlands for investigating water and sediment fluxes in catchment, channel and reach.” *Journal of Hydrology and Hydromechanics* 61: 334–346.

Luoma, S. N., and Rainbow, P. S. 2005. “Why is metal bioaccumulation so variable? Biodynamics as a unifying concept.” *Environmental Science & Technology* 39(7): 1921–1931. doi:10.1021/es048947e

MacDonald, D. D., Ingersoll, C. G., and Berger, T. A. 2000. “Development and evaluation of consensus-based sediment quality guidelines for freshwater ecosystems.” *Archives of Environmental Contamination and Toxicology* 39: 20–31.

Mathews, T. J., Looney, B. B., Bryan, A. L., Smith, J. G., Miller, C. L., Southworth, G. R. and Peterson, M. J. 2015. “The effects of a stannous chloride-based water treatment system in a mercury contaminated stream.” *Chemosphere* 138: 190–196.

Mistry, R., and Ackerman, J. D. 2018. “Flow, flux, and feeding n freshwater mussels.” *Water Resources Research* 54(10): 7619–7630. https://doi.org/10.1029/2018wr023112

Mathews, T., Southworth, G., Peterson, M., Roy, W. K., Ketelle, R., Valentine, C., and Gregory, S. 2013. “Decreasing aqueous mercury concentrations to achieve safe levels in fish: Examining the water-fish relationship in two point-source contaminated streams.” *Science of the Total Environment* 443: 836–843.

Mukherjee, A., Das, S., Bhattacharya, T., De, M., Maiti, T., and Kumar De, T. 2014. “Optimization of phytoplankton preservative concentrations to reduce damage during long-term storage.” *Biopreservation and Biobanking* 12: 139–147.

Muller, K. A., and Brooks, S. C. 2019a. “Effectiveness of sorbents to reduce mercury methylation.” *Environmental Engineering Science* 36(3): 361–371.

Muller, K. A., Brandt, C. C., Mathews, T. J., and Brooks, S. C. 2019b. "Methylmercury sorption onto engineered materials." *Journal of Environmental Management* 245: 481–488. doi.org/10.1016/j.jenvman.2019.05.100 (data DOI: 10.17632/jcfwd5sg4w.1)

Murphy, S., Schwartz, G. E., and Brooks, S. C. In review. "Demethylation or sorption? The fate of methylmercury in the presence of manganese dioxide." *Environmental Engineering Science*.

Olsen, T., Muller, K. A., Painter, S. L., and Brooks, S. C. 2018. "Kinetics of Methylmercury Production Revisited." *Environmental Science & Technology* 52(4): 2063–2070. doi: 10.1021/acs.est.7b05152.

Olsen, T. A., Brandt, C. C., and Brooks, S. C. 2016. "Periphyton biofilms influence net methylmercury production in an industrially contaminated system." *Environmental Science & Technology* 50(20): 10843–10850. doi: 10.1021/acs.est.6b01538.

Olivera, F., Valenzuela, M., Srinivasan, R., Choi, J., Cho, H., Koka, S., and Agrawal, A. 2006. "ArcGIS-SWAT: A geodata model and GIS interface for SWAT." *Journal of the American Water Resources Association* 42(2): 295–309.

Paulson, K. M. A. 2014. "Methylmercury Production in Riverbank Sediments of the South River, Virginia (USA) and Assessment of Biochar as a Mercury Treatment Option." Thesis, University of Waterloo, Waterloo, Ontario. http://hdl.handle.net/10012/8213

Paulson, K. M. A., Ptacek, C. J., Blowes, D. W., Gould, W. D., Ma, J., Landis, R. C., and Dyer, J. A. 2018. "Role of Organic Carbon Sources and Sulfate in Controlling Net Methylmercury Production in Riverbank Sediments of the South River, VA (USA)." *Geomicrobiology Journal* 35(1): 1–14.

Pena, E. A., and Slate, E. H. 2006. "Global Validation of Linear Model Assumptions," *Journal of the American Statistical Association* 101(473): 341–354.

Peterson, M. J., Looney, B., Southworth, G., Eddy-Dilek, C., Watson, D., Ketelle, R., and Bogle, M. 2011. *Conceptual Model of Primary Mercury Sources, Transport Pathways, and Flux at the Y-12 Complex and Upper East Fork Poplar Creek, Oak Ridge, Tennessee.* ORNL/TM-2011/75. Oak Ridge National Laboratory, Oak Ridge, Tennessee.

Peterson, M. J., Brooks, S. C., Mathews, T. J., Mayes, M. A., Johs, A., Watson, D. B., Poteat, M. D., and Pierce, E. 2015. *Mercury Remediation Technology Development for Lower East Fork Poplar Creek.* ORNL/SPR-2014/645. Oak Ridge National Laboratory, Oak Ridge, Tennessee.

Peterson, M. J., et al. 2018. *Mercury Remediation Technology Development for Lower East Fork Poplar Creek—2017 Progress Report.* ORNL/TM-2017/480. Oak Ridge National Laboratory, Oak Ridge, Tennessee.

Pouil, S., Hills, A., and Mathews, T. In review. "The effects of food quantity, light, and temperature on clearance rates in freshwater bivalves (Cyrenidae and Unionidae)." *Hydrobiologia*.

R Core Team. 2019. "R: A language and environment for statistical computing." *R Foundation for Statistical Computing*, Vienna, Austria. http://www.r-project.org/index.html

Riisgård, H. U. 2001. "On measurement of filtration rates in bivalves—the stony road to reliable data: review and interpretation." *Marine Ecology Progress Series* 211: 275–291.

Riscassi, A. L., Miller, C., and Brooks, S. C. 2016. "Seasonal and flow-driven dynamics of particulate and dissolved mercury and methylmercury in a stream impacted by an industrial mercury source." *Environmental Toxicology and Chemistry* 35(6): 1386–1400. doi:10.1002/etc.3310.

Riva-Murray, K., Bradley, P. M., Scudder Eikenberry, B. C., Knightes, C. D., Journey, C. A., Brigham, M. E., and Button, D. T. 2013. "Optimizing Stream Water Mercury Sampling for Calculation of Fish Bioaccumulation Factors." *Environmental Science & Technology* 47: 5904–5912.

Ryon, M. G., Stewart, A. J., Kszos, L. A., and Phipps, T. L. 2002. "Impacts on streams from the use of sulfur-based compounds for dechlorinating industrial effluents." *Water Air and Soil Pollution* 136: 255–268.

Salerno, J., Gillis, P. L., Bennett, C. J., Sibley, P. K., and Prosser, R. S. 2018. "Investigation of clearance rate as an endpoint in toxicity testing with freshwater mussels (Unionidae)." *Ecotoxicology and Environmental Safety* 163: 165–171. https://doi.org/10.1016/j.ecoenv.2018.07.054

Simon, A., Curini, A., Darby, S. E., and Langendoen, E. J. 2000. “Bank and near-bank processes in an incised channel.” *Geomorphology* 35(3–4): 193–217.

Southworth, G., Peterson, M., and Bogle, M. 2004. “Bioaccumulation factors for mercury in stream fish.” *Environmental Practice* 6: 135–143. https://www.fs.fed.us/eng/pubs/pdf/05231301.pdf

Thornton, P. E., Thornton, M. M., Mayer, B. W., Wei, Y., Devarakonda, R., Vose, R. S., and Cook, R. B. 2018. *Daymet: Daily surface weather data on a 1-km grid for North America, Version 3*. Oak Ridge National Laboratory Distributed Active Archive Center, Oak Ridge, Tennessee. https://doi.org/10.3334/ORNLDAAC/1328

Tom, K. R., Newman, M. C., and Schmerfeld, J. 2010. “Modeling mercury biomagnification (South River, Virginia, USA) to inform river management decision making.” *Environmental Toxicology and Chemistry* 29(4): 1013–1020. doi: 10.1002/etc.117.

Trudel, M., and Rasmussen, J. B. 1997. “Modeling the Elimination of Mercury by Fish.” *Environmental Science & Technology* 31: 1716–1722.

Tsui, M. T. K., Findlay, J. C., Balogh, S. J., and Nollet, Y. H. 2010. “In situ production of methylmercury within a stream channel in northern California.” *Environmental Science & Technology* 44: 6998–7004.

Turner, R. R., and Southworth, G. R. 1999. *Mercury Contaminated Sites*. R. Ebinghaus, R. R. Turner, L. De Lacerda, O. Vasiliev, and W. Salomons, Eds. Berlin: Springer-Verlag.

Ward, D. M., Nislow, K. H., Chen, C. Y., and Folt, C. L. 2010. “Rapid, Efficient Growth Reduces Mercury Concentrations in Stream-Dwelling Atlantic Salmon.” *Transactions of the American Fisheries Society* 139: 1–10.

Watson, D., Bevelheimer, M., Brandt, C., DeRolph, C., Brooks, S., Mayes, M., Olsen, T., Dickson, J., Peterson, M., and Ketelle, R. 2017. *Evaluation of lower East Fork Poplar Creek mercury sources–Model update*. ORNL/SR-2016/503. Oak Ridge National Laboratory, Oak Ridge, Tennessee.

Watson, D., Brooks, S., Mathews, T., Bevelheimer, M., DeRolph, C., Brandt, C., Peterson, M., and Ketelle, R. 2016. *Evaluation of lower East Fork Poplar Creek mercury sources.* ORNL/TM-2016/134. Oak Ridge National Laboratory, Oak Ridge, Tennessee.

USDA-NRCS (US Department of Agriculture Natural Resources Conservation Service). 2006. *US General Soil Map (STATSGO2)*. Natural Resources Conservation Service. http://dx.doi.org/10.15482/USDA.ADC/1242480.

Vlassopoulos, D., Kanematsu, M., Henry, E. A., Goin, J., Leven, A., Glaser, D., Brown, S. S., and O’Day, P. A. 2018. “Manganese(iv) oxide amendments reduce methylmercury concentrations in sediment porewater.” *Environmental Science: Process & Impacts* 20: 1746–1760.

Waples, J. S., Nagy, K. L., Aiken, G. R., and Ryan, J. N. 2005. “Dissolution of cinnabar (HgS) in the presence of natural organic matter.” *Geochimica et Cosmochimica Acta* 69: 1575–1588.